

THE UNIVERSITY OF TENNESSEE
SPACE INSTITUTE

DOE/ET/10815-232
DIST. CATEGORY UC-112
UTSI 95/05

SUPERHEATER/INTERMEDIATE TEMPERATURE AIR HEATER
TUBE CORROSION TESTS
IN THE MHD COAL FIRED FLOW FACILITY
(MONTANA ROSEBUD POC TESTS)

January 1996

Report Prepared by

M. White

The University of Tennessee Space Institute
Energy Conversion Research and Development Programs
Tullahoma, Tennessee 37388

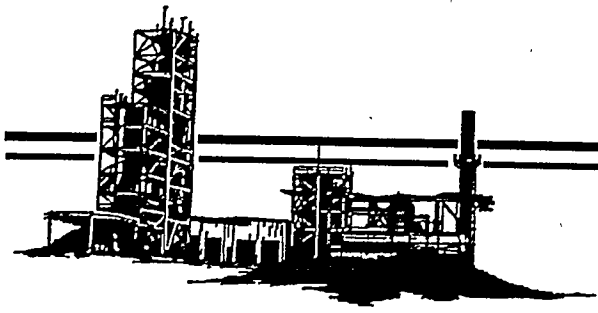
for

THE UNITED STATES DEPARTMENT OF ENERGY
Under Contract No. DE-AC02-79ET10815

TULLAHOMA, TENNESSEE 37388-8897

DISTRIBUTION OF THIS DOCUMENT IS UNLIMITED

MASTER



COAL FIRED FLOW FACILITY

"This report was prepared as an account of work sponsored by the United States Government. Neither the United States nor the United States DOE, nor any of their employees, nor any of their contractors, subcontractor, or their employees, makes any warranty, express or implied, or assumes any legal liability or responsibility for the accuracy, completeness, or usefulness of any information, apparatus, product or process disclosed, or represents that its use would not infringe privately owned rights."

TULLAHOMA, TENNESSEE 37388-8897

DOE/ET/10815-232
DIST. CATEGORY UC-112
UTSI 95/05

SUPERHEATER/INTERMEDIATE TEMPERATURE AIR HEATER
TUBE CORROSION TESTS
IN THE MHD COAL FIRED FLOW FACILITY
(MONTANA ROSEBUD POC TESTS)

January 1996

Report Prepared by

M. White

The University of Tennessee Space Institute
Energy Conversion Research and Development Programs
Tullahoma, Tennessee 37388

for

THE UNITED STATES DEPARTMENT OF ENERGY
Under Contract No. DE-AC02-79ET10815

MASTER

DISTRIBUTION OF THIS DOCUMENT IS UNLIMITED *DL*

TABLE OF CONTENTS

	<u>Page</u>
LIST OF FIGURES	iv
LIST OF TABLES	v
ABSTRACT	1
INTRODUCTION	2
BACKGROUND	2
TEST CONDITIONS	4
SAMPLING AND EVALUATION PROCEDURES	11
Measurement of Wall Thickness Change	11
Measurement of Corrosion Scale Thickness and Internal Penetration Depth	14
Scale Morphology Evaluation	14
RESULTS	14
Scaling and Penetration	14
Scaling and Penetration vs. Metal Temperature	17
Scale and Penetration Morphology Description	22
Wall Thinning Data	31
DISCUSSION	34
SUMMARY AND CONCLUSIONS	35
ACKNOWLEDGEMENT	39
REFERENCES	39

LIST OF FIGURES

	<u>Page</u>
1. CFFF integrated MHD bottoming cycle schematic.	4
2. Placement of test alloys in TS1 and TS2.	8
3. Placement of test alloys in TS3.	9
4. Locations of tube metal thermocouples.	10
5. Typical distributions of metal temperature for LMF5 test section tubes.	12
6. Corrosion scale thickness and penetration depth (in micrometers) for CFFF superheater/ITAH tubes exposed to 991 test hours (except as noted) under LMF5 conditions.	15
7. Average scale thickness and penetration depth for alloys in Pass 2 of TS1 and TS2. . .	17
8. Scale thickness for TS1 alloys as a function of average exposure temperature.	18
9. Scale thickness for TS2 alloys as a function of average metal temperature.	19
10. Penetration depth for TS1 alloys as a function of average metal temperature.	20
11. Penetration depth for TS2 as a function of average exposure temperature.	21
12. Scale and penetration morphology for alloys of TS1 pass 1.	23
13. Scale and penetration morphology for alloys of TS2 pass 1.	24
14. Scale and penetration morphologies for alloys of TS1 pass 2.	25
15. Scale and penetration morphologies for alloys of TS2 pass 2.	26
16. Fireside tube surface recession (micrometers) (averaged at a given cross-section) plotted against average metal exposure temperature (°F).	32
17. More fireside tube recession (micrometers) (averaged at a given cross-section) plotted against average metal exposure temperature (°F).	33

LIST OF TABLES

	<u>Page</u>
1. Alloys and nominal sizes of tested materials.	6
2. Nominal composition of test alloys (in weight percent).	7
3. Time average inlet gas temperatures to test sections for each run (°F)	10
4. Average tube metal temperatures at measurement locations (°F).	13
5. Comparison of average corrosion rates (mm/yr) in LMF5 tests with Montana Rosebud coal to LMF4 tests with Illinois #6 coal.	36

SUPERHEATER/INTERMEDIATE TEMPERATURE AIR HEATER
TUBE CORROSION TESTS IN THE MHD COAL FIRED FLOW FACILITY
(MONTANA ROSEBUD POC TESTS)*

M. White

ABSTRACT

Nineteen alloys have been exposed for approximately 1000 test hours as candidate superheater and intermediate temperature air heater tubes in a U.S. DOE facility dedicated to demonstrating Proof of Concept for the bottoming or heat and seed recovery portion of coal fired magnetohydrodynamic (MHD) electrical power generating plants. Corrosion data have been obtained from a test series utilizing a western United States sub-bituminous coal, Montana Rosebud. The test alloys included a broad range of compositions ranging from carbon steel to austenitic stainless steels to high chromium nickel-base alloys. The tubes, coated with K_2SO_4 -containing deposits, developed principally oxide scales by an oxidation/sulfidation mechanism. In addition to being generally porous, these scales were frequently spalled and/or non-compact due to a dispersed form of outward growth by oxide precipitation in the adjacent deposit. Austenitic alloys generally had internal penetration as transgranular and/or intergranular oxides and sulfides. While only two of the alloys had damage visible without magnification as a result of the relatively short exposure, there was some concern about long-term corrosion performance owing to the relatively poor quality scales formed. Comparison of data from these tests to those from a prior series of tests with Illinois #6, a high sulfur bituminous coal, showed less corrosion in the present test series with the lower sulfur coal. Although K_2SO_4 was the principal corrosive agent as the supplier of sulfur, which acted to degrade alloy surface scales, tying up sulfur as K_2SO_4 prevented the occurrence of complex alkali iron trisulfates responsible for severe or catastrophic corrosion in conventional power plants with certain coals and metal temperatures.

*Research sponsored by the U. S. Department of Energy under Contract No. DE-AC02-79ET10815

INTRODUCTION

Demonstration of technology to allow design and operation of the bottoming portion of MHD electrical power generating plants requires corrosion testing of materials of construction for critical hot gas path components including superheaters, reheaters, and air heaters under conditions as prototypical as possible. Such tests have been conducted in the DOE Coal Fired Flow Facility (CFFF) at The University of Tennessee Space Institute (UTSI) as part of the National MHD Program. A two thousand hour exposure of tube materials with firing of an eastern high sulfur coal, Illinois #6, was conducted as part of a test series denoted LMF4.¹ Subsequently, a series of exposures totaling approximately one thousand hours designated LMF5 was conducted firing western low sulfur, high ash Montana Rosebud coal. Results of corrosion evaluations from that test series are presented in this report.

BACKGROUND

A coal-fired, open-cycle MHD plant would consist of an MHD topping unit and a steam bottoming system that is similar to the steam generator in a conventional power plant. The combustion gas, after passing through the MHD channel and diffuser, would enter the steam bottoming plant at a temperature (3500-3800°F) somewhat higher than the maximum flame temperature in conventional plants, in a fuel-rich condition (stoichiometric ratio ~ 0.85), and with a larger quantity of condensible solids resulting from the addition in the combustor of a potassium gas seeding compound such as potassium carbonate. The first component of a typical bottoming plant into which the combustion gas would pass is the radiant furnace, which is a large chamber with tubular boiler water-walls similar to the furnace of a conventional plant. The walls of the MHD radiant boiler would probably be refractory lined, however, to resist corrosion from the reducing, sulfur-containing flue gas. This type of construction would be similar to that used in conventional boilers with slagtap design. Secondary combustion of the gas would be performed by injecting heated air at a location toward the downstream end of the radiant furnace. Beyond the secondary combustion zone would be tubular heat exchanger components, primarily radiative initially and

convective further downstream, which would superheat and reheat steam, preheat combustion air, and heat boiler feed water.

Because of the large amount of seed material, mostly as K_2SO_4 and K_2CO_3 , in the combustion gas, the solids deposition conditions in the convective sections would be considerably different from those encountered in conventional coal burning plants, including those that burn coals having a highly alkaline ash. The form of deposits collected on tube surfaces would vary depending on gas temperature. In the hottest regions, above the seed melting point, hard sintered deposits would occur with a thin, low viscosity, flowing liquid seed surface film. Those deposits might be quite thick and massive owing to the high collection efficiency of the wet surface and the difficulty of removal. In regions just below the seed melting point, deposits would still be sintered, but not as thick. With lowering gas temperature, next would come a region of partially consolidated and sintered deposits, and then finally totally unsintered, powdery deposits.

Corrosion of tube metals will occur by interaction with both the deposit and the combustion gas. Natesan² showed the active deposit species to be K_2SO_4 , and that corrosion is substantially greater with deposits than without. While compact, protective oxide scales will be produced on appropriately chosen heat resisting alloys exposed solely to oxidizing combustion gases, the presence of sulfate salt deposits will change the corrosion mechanism from purely oxidation to oxidation/sulfidation, which is a synergistic process.

While the liquid phase alkali iron trisulfates which can be formed under certain conditions and cause catastrophic tube corrosion in conventional coal ash corrosion have not been found and are not expected in coal-fired MHD due to insufficient SO_3 , linear corrosion rates of alloys with up to 25% Cr from test exposures of 2000 hours in the CFFF with deposits derived from burning seeded Illinois #6 coal were still more than 0.5 mm/yr at 1400°F.¹ By parabolic kinetics, however, alloy 310 had less than 0.5 mm/yr corrosion at 1400°F, while the 18-8 stainless steels were variably above and below 0.5 mm/yr at 1100°F. Alteration of scale by dissolved sulfur and by sulfides, transfer of metal from the surface scale into the deposit, and thermal and physical stresses from load changes and sootblowing all contributed to the occurrence of relatively nonprotective scales.

TEST CONDITIONS

LMF5 tube material corrosion testing was conducted during six test runs denoted LMF5E through J with individual on-coal and on-seed run times of 38.6, 287.6, 312.9, 87.6, 207.4, and 51.3 hours totaling 985.4 hours. Montana Rosebud coal was fired at 85% stoichiometry in the primary combustor at a nominal 20 MW thermal. Potassium carbonate was injected as a 47% solution to seed the flow with 1% potassium by weight for a nominal K_2/S ratio of 4.4. Within the downstream portion of the radiant furnace, heated secondary combustion air was added to bring the stoichiometry to 105%. Solid or solidifiable species exiting the radiant furnace consisted mostly of flyash, K_2SO_4 , and K_2CO_3 in approximately equal amounts. Tube metals for corrosion testing were located downstream of the radiant furnace in three rectangular cross section duct modules termed "test sections (TS)" as depicted in Figure 1. TS1, TS2, and TS3 were in successively lower gas temperature regimes, chosen to simulate critical service regimes expected in an MHD retrofit plant, and accomplished by the introduction of water-cooled tube bundles between the test sections.

Each Test Section tube bundle consisted of eight pendant, in-line, u-shaped tubes on 6 inch by 6 inch centers. TS1 and TS2 tubes were single u-bends, so that there were eight tubes across the

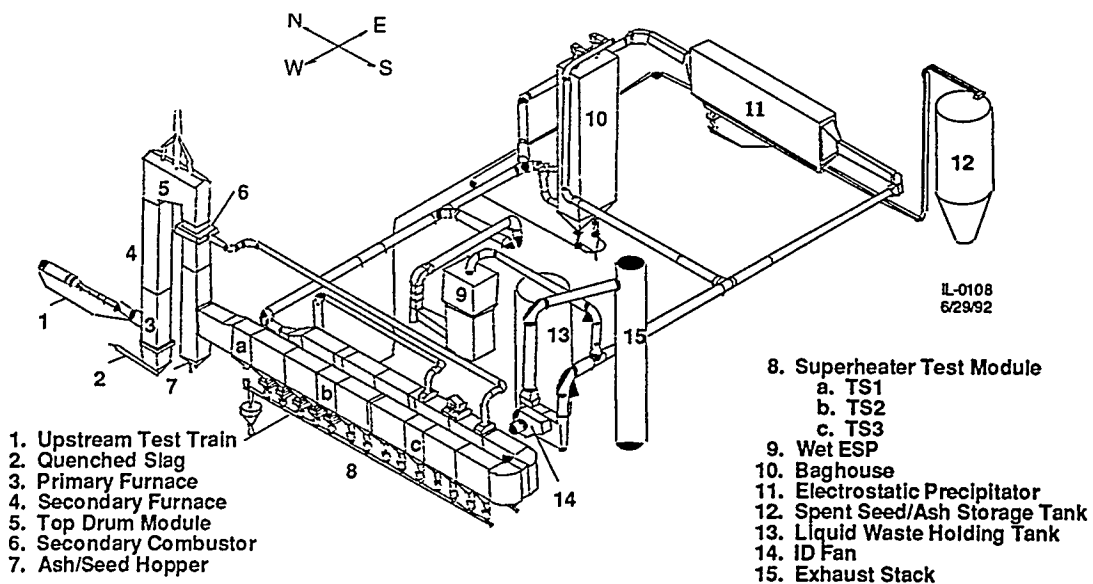


Figure 1. CFFF integrated MHD bottoming cycle schematic.

duct and two passes deep in the flow direction. TS3 tubes were double u-bends, giving eight tubes across and four deep. Each tube was about 8 feet long (7 feet within the duct) and individually removable, having its own tube sheet which bolted and sealed into a rectangular opening in the roof of the duct. The tubes of each Test Section were manifolded outside the duct to inlet and outlet steam headers. Low pressure (130 psig) steam from a package boiler was used for cooling the tubes, and was vented to the atmosphere from the outlet headers.

Tube materials and nominal sizes tested are given in Table 1. Because of limited availability of tubes in the 1.5 inch diameter desired, tubes (or pipes) ranging from 1.315 inches to 2.24 inches were used. Where multiple alloys were used in a single u-bend, they were welded together with appropriate filler metals. Nominal compositions of alloys tested are given in Table 2. Tube alloys and their placement were the same for TS1 and TS2, while those in TS3 were different. TS1 and TS2 contained wrought austenitic stainless steels and more highly alloyed heat resisting iron or nickel-based alloys as candidates for ITAH usage at temperatures to 1400°F or for steam superheater/reheater usage to 1100°F metal temperatures. TS3 alloys included carbon steel, low and intermediate chromium steels, and 18-8 stainless steels for candidate service in a superheater or for the intermediate or transition portion of the ITAH at metal temperatures to 1100°F. Figure 2 shows the placement of TS1 and TS1 alloys, and Figure 3 shows the placement of alloys in TS3.

Deposits on TS1 tubes were analyzed and found to consist of an average of 30% K_2SO_4 , 35% K_2CO_3 , and 35% flyash, those on TS2 of 36% K_2SO_4 , 40% K_2CO_3 , and 24% flyash, and those on TS3 of 26% K_2SO_4 , 39% K_2CO_3 , and 35% flyash. However, the deposit directly adjacent to the surface of tubes contained considerably less flyash. Owing to the minor amount and inertness of flyash in deposits near the tube surfaces, the corrosive effect was equivalent to that of the salt alone. The presence of potassium carbonate, which is highly hygroscopic, in the deposits made it necessary to enclose and seal the tubes with plastic "bags" between tests to avoid moisture absorption.

Average inlet gas temperatures for the three test sections are given in Table 3, being about 2200°F for TS1, 1600°F for TS2, and 1277°F for TS3. Thermocouples in weld pads on the tube

Table 1. Alloys and nominal sizes of tested materials.

Tube #	alloy	Size	Wall (in)
TS1-1C	556/316H	1" Pipe/1.5" Tube	Sch.10 (0.109)/(0.120)
TS1-2C	RA85H/HR-160 /253MA	1" Pipe/1" Pipe/1" Pipe	Sch.40 (0.133)/Sch.10 (0.133)/Sch.40 (0.133)
TS1-3C	HR3C/347H	2.24" Tube/1.5" Tube	(0.157)/(0.156)
TS1-4C	CR30A/304H	1.5" Tube/1.5" Tube	(0.250)/(0.165)
TS1-5C	IN 690/310	1.9" Tube/1.25" Pipe	(0.200)/Sch.40 (0.140)
TS1-6C	CR35A/310	1.5" Tube/1.25" Pipe	(0.250)/Sch.40 (0.140)
TS1-7C	cr-800H/cr-T91	1.5" Tube/2.0" Tube	(0.134)/(0.320)
TS1-8C	MA956/347H	1.9" Tube/1.5" Tube	(0.200)/(0.156)
TS2-1C	556/316H	1" Pipe/1.5" Tube	Sch.10 (0.109)/(0.120)
TS2-2C	RA85H/HR-160/ 253MA	1" Pipe/1" Pipe/1" Pipe	Sch.40 (0.133)/Sch.10 (0.133)/Sch.40 (0.133)
TS2-3C	HR3C/347H	2.24" Tube/1.5" Tube	(0.157)/(0.156)
TS2-4C	CR30A/304H	1.5" Tube/1.5" Tube	(0.250)/(0.165)
TS2-5C	IN 690/310	1.9" Tube/1.25" Pipe	(0.200)/Sch.40 (0.140)
TS2-6C	CR35A/310	1.5" Tube/1.25" Pipe	(0.250)/Sch.40 (0.140)
TS2-7C	cr-800H/cr-T91	1.5" Tube/2.0" Tube	(0.134)/(0.320)
TS2-8C	MA956/347H	1.9" Tube/1.5" Tube	(0.200)/(0.156)
TS3-1C	316H/SA192	1.5" Tube/1.5" Tube	(0.120)/(0.165)
TS3-2C	347H/T11	1.5" Tube/1.5" Tube	(0.156)/(0.180)
TS3-3C	T22	1.5" Tube	(0.150)
TS3-4C	T91	2.0" Tube	(0.320)
TS3-5C	T91	2.0" Tube	(0.320)
TS3-6C	T22	1.5" Tube	(0.150)
TS3-7C	347H/T11	1.5" Tube/1.5" Tube	(0.156)/(0.180)
TS3-8C	304H/SA192	1.5" Tube/1.5" Tube	(0.165)/(0.165)

Table 2. Nominal composition of test alloys (in weight percent).

	Cr	Ni	Cr/Ni	Fe	Mo	W	V	Nb	Ti	Mn	Si	P	S	Al	C	N
SA192	-	-	-	Bal.	-	-	-	-	-	0.45	0.20	0.03	0.03	-	0.15	-
T11	1.25	-	-	Bal.	0.50	-	-	-	-	0.45	0.75	0.03	0.03	-	0.15	-
T22	2.50	-	-	Bal.	1.00	-	-	-	-	0.45	0.50	0.03	0.03	-	0.15	-
T9	9.00	-	-	Bal.	1.00	-	-	-	-	0.45	0.40	0.03	0.03	-	0.15	-
316	17.0	12.0	1.42	Bal.	2.50	-	-	-	-	2.00	1.00	0.05	0.03	-	0.07	-
347	18.0	11.0	1.64	Bal.	-	-	-	0.70	-	2.00	1.00	0.05	0.03	-	0.07	-
RA85H	18.0	14.0	1.29	Bal.	-	-	-	-	-	0.50	3.50	-	-	1.00	-	-
304H	19.0	9.00	2.11	Bal.	-	-	-	-	-	2.00	1.00	0.05	0.03	-	0.07	-
MA 956	20.0	-	-	Bal.	-	-	-	0.50	-	-	-	-	-	4.50	-	-
800H	21.0	32.5	0.65	Bal.	-	-	-	-	0.38	0.80	0.50	-	-	0.38	0.08	-
253MA *	21.0	11.0	1.91	Bal.	-	-	-	-	-	0.80	1.70	0.04	0.03	-	0.10	0.17
Temp A3	22.0	15.0	1.47	Bal.	-	-	-	0.70	-	1.37	0.40	0.03	0.01	-	0.05	0.19
556 **	22.0	20.0	1.10	Bal.	3.00	2.50	-	-	-	1.00	0.40	-	-	0.20	0.10	0.20
310	25.0	20.0	1.25	Bal.	-	-	-	-	-	2.00	1.50	0.05	0.03	-	0.25	-
HR3C	25.0	20.0	1.25	Bal.	-	-	-	***	-	2.00	1.50	0.05	0.03	-	0.08	0.10
HR-160 *	28.0	Bal.	0.74	4.0	-	-	-	-	-	0.50	2.75	-	-	-	0.05	-
IN 690	29.0	Bal.	0.47	9.0	-	-	-	-	-	-	-	-	-	-	-	-
CR30A	30.5	Bal.	0.62	17.7	2.10	-	-	-	0.18	0.20	0.27	-	-	0.14	0.06	-
CR35A	35.0	Bal.	0.76	18.2	-	-	-	0.50	-	-	0.07	-	-	-	0.07	-

* Contains 0.05% Ce ** Contains 18.0% Co, 0.6% Ta, 0.02% La, 0.02% Zr *** 1% Nb+Ta # Contains 27% Co

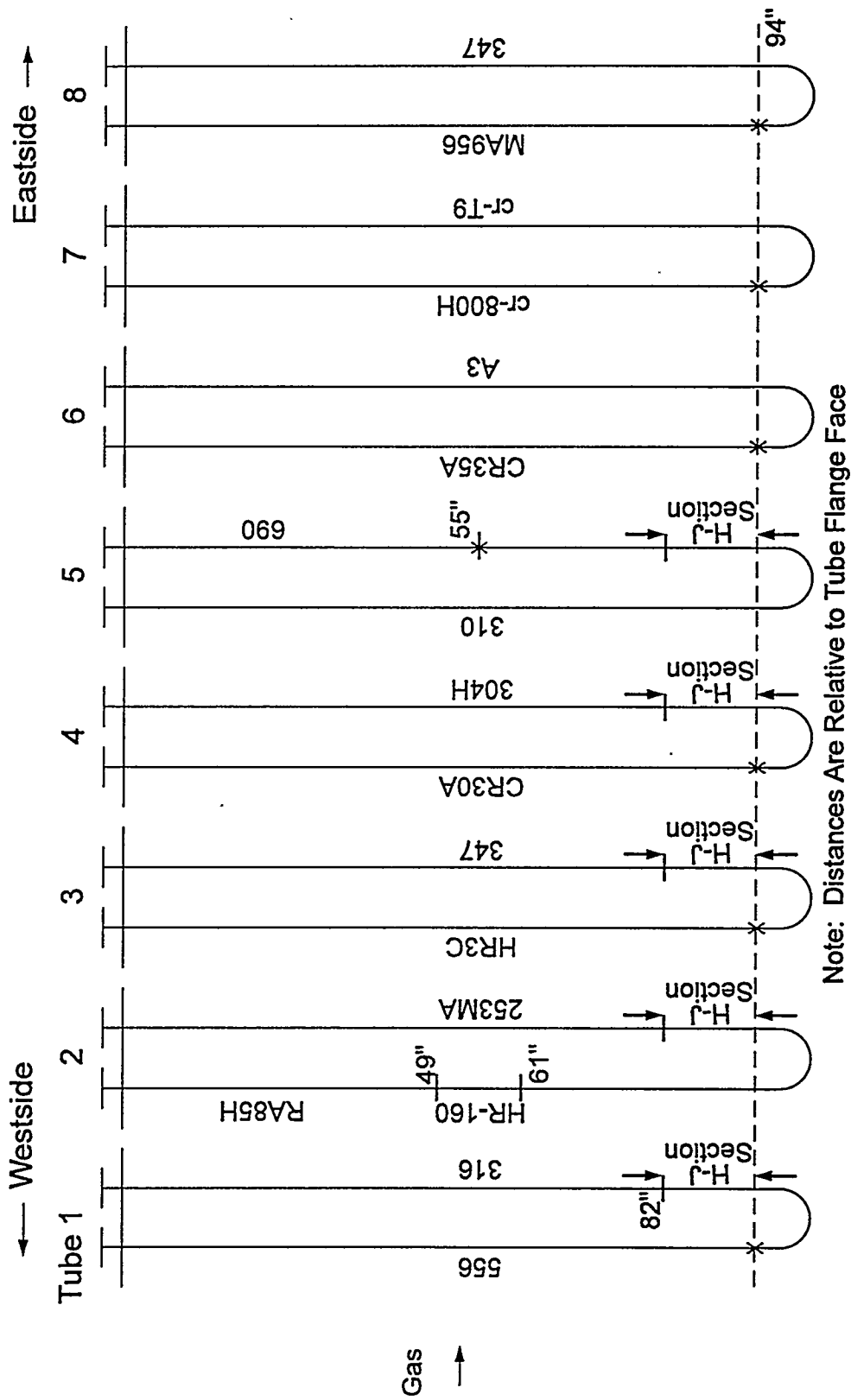
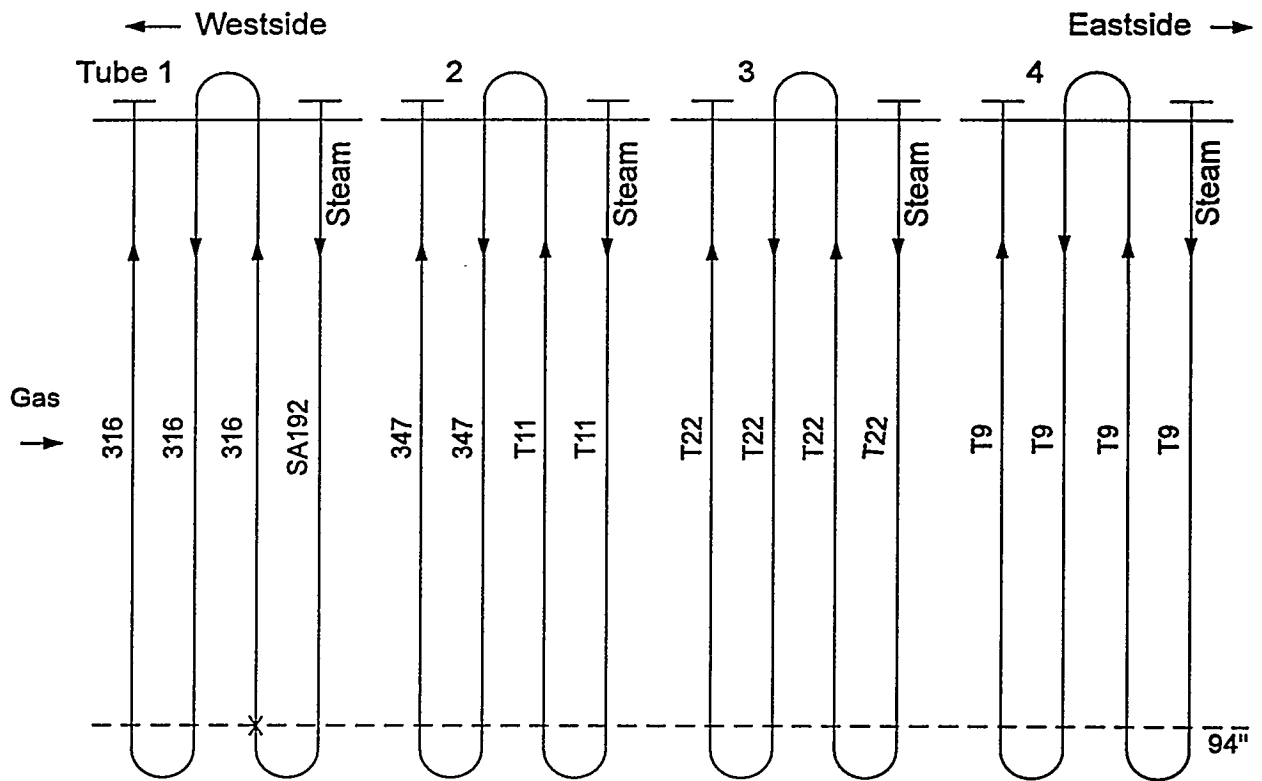


Figure 2. Placement of test alloys in TS1 and TS2.



Note: Distances Are Relative to Tube Flange Face

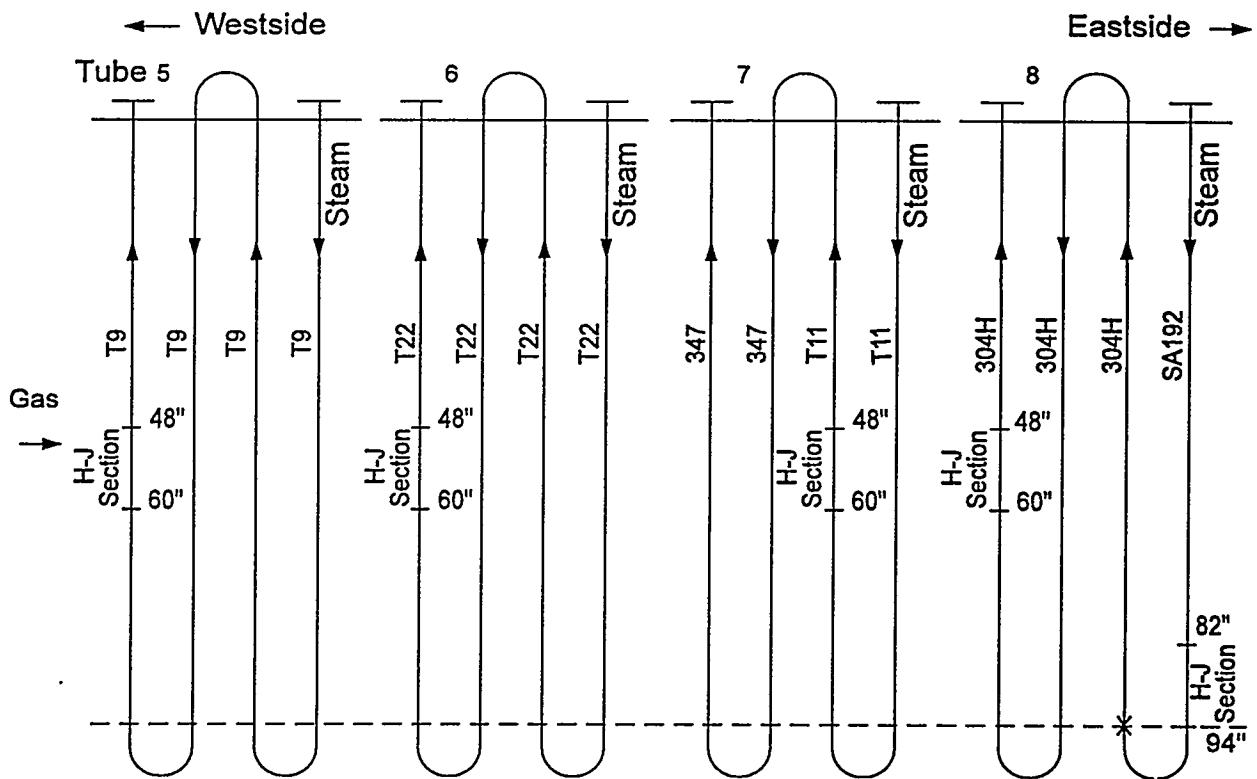


Figure 3. Placement of test alloys in TS3.

Table 3. Time Average Inlet Gas Temperatures to Test Sections for Each Run (°F)

LMF5	E	F	G	H	I	J	Average
TS1	1912	2144	2028	2036	2046	1827	1998.83
TS2	1530	1698	1659	1598	1634	1436	1592.5
TS3	1229	1339	1337	1297	1295	1165	1277

Note: Values are uncorrected for thermocouple radiation loss. Actual TS1 gas temperatures would be about 200°F higher.

outer surfaces at the locations shown in Figure 4 were used to monitor and control tube temperatures. In TS1 and TS2, tubes 1 and 4 had surface thermocouples on the leading edge at positions A-E in the figure. Tubes 5 and 8 had thermocouples at the same places, but at the trailing edge. Tubes 2 and 3 had a thermocouple at position D only, at the leading edge. In TS3, tube 4 had surface thermocouples on the leading edge at positions A-J. Tubes 1, 2, and 3 had thermocouples at positions B and I at the leading edge. There were no trailing edge thermocouples on TS3. Steam

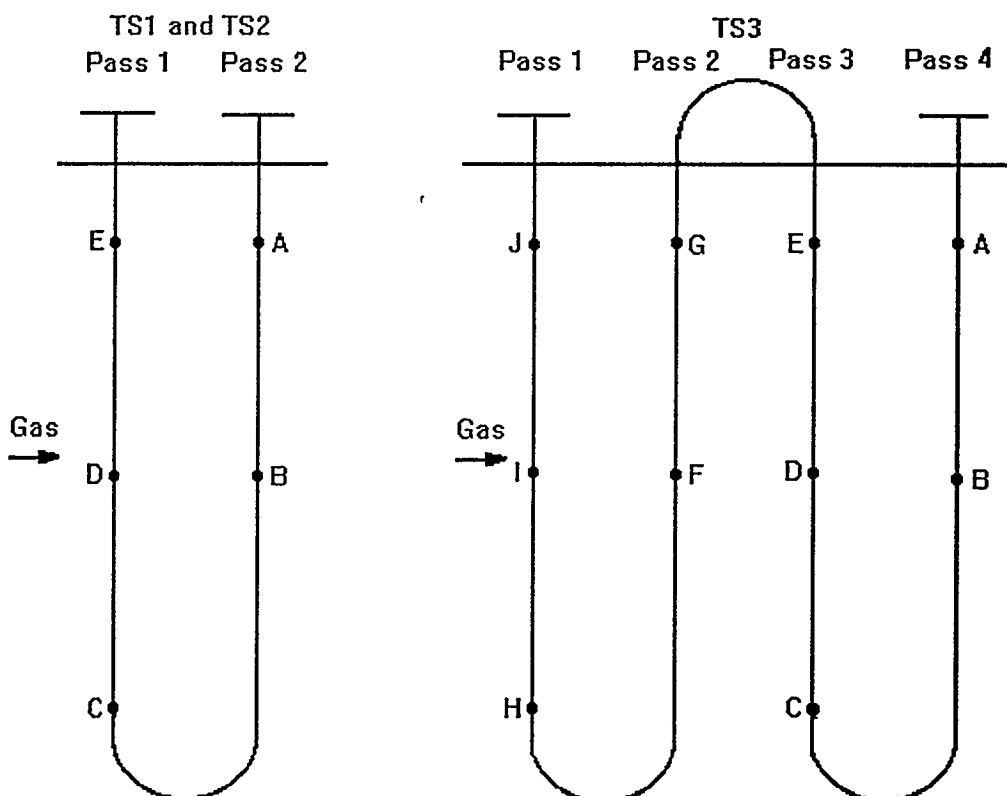


Figure 4. Locations of tube metal thermocouples.

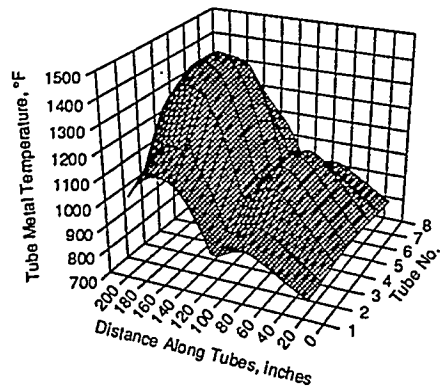
flow to the supply header for each test section was varied under either automatic or manual control to maintain prescribed temperatures at the hottest locations within $\pm 50^{\circ}\text{F}$. These prescribed maximum metal temperatures were 1400°F for TS1 and TS2 and 1100°F for TS3. The averaged and smoothed distributions of metal temperatures over the test sections are shown in 3-D plots in Figure 5. The x-axis label of the plots refers to the distance along the tubes from the steam inlet flange to the steam outlet flange. Temperatures were assumed to be symmetrical about the axial centerline of the duct. A large lateral gradient in temperature was present only at the TS1 leading edge. A tabulation of temperatures from those distributions at one foot intervals along the leading edge is given in Table 4. "Elevation" in that table refers to the vertical distance downward from the flange face for that pass.

SAMPLING AND EVALUATION PROCEDURES

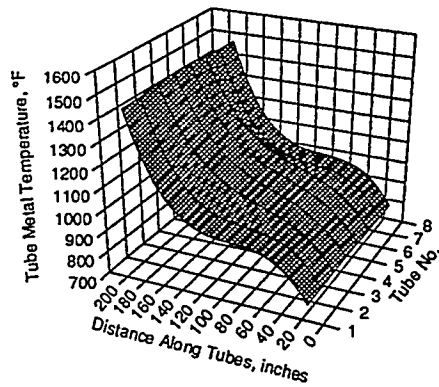
Two methodologies of quantitative corrosion evaluation were employed, one being measurement of tube wall thickness change and the other being measurement of corrosion scale thickness and internal penetration depth.

Measurement of Wall Thickness Change

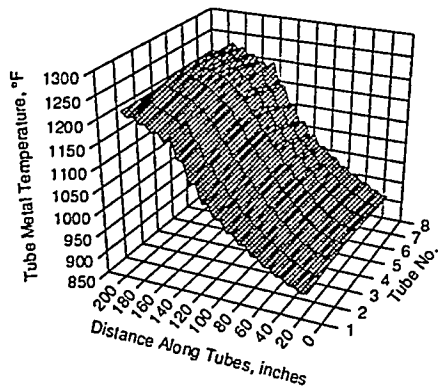
Pre-exposure wall thickness measurements were made by ultrasonic gauging at locations defined as to distance from the top end of the tube and angle relative to the leading edge of the tube. For TS1 and TS2, post-exposure wall thicknesses were measured either by a dial displacement gauge affixed to an optical microscope stage and using polished cross-sectional samples taken at locations of pre-exposure measurements or by use of a "tubing" or "inside" micrometer on tube pieces cut such that pre-exposure measurement locations were one half inches from one end and, thus, could be remeasured. Polished sections were taken from 8 locations on each tube, and three measurements were made from each section. Micrometer measurements were made at six cross sectional locations and at 8 angular positions (every 45 degrees) at each section. Prior to micrometer measurement, the outer surface of tube pieces was glass bead blasted for removal of corrosion scale (but essentially no metal). Seventy-two wall thickness change measurements were made for each tube of TS1 or TS2. TS3 remaining wall measurements were made ultrasonically.



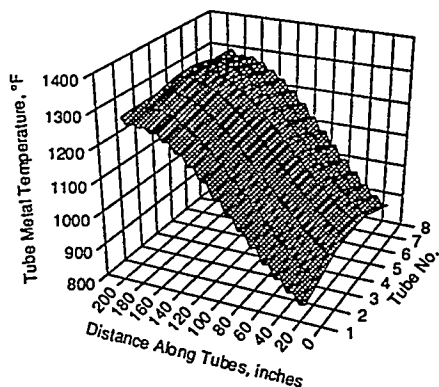
a. TS1 Leading Edge



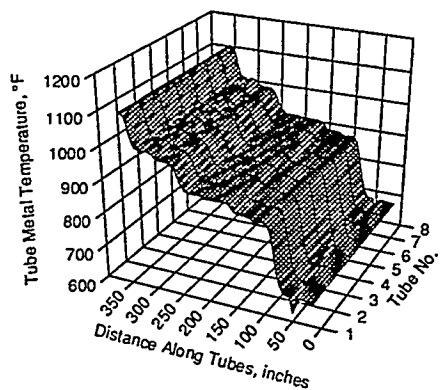
b. TS1 Trailing Edge



c. TS2 Leading Edge



d. TS2 Trailing Edge



e. TS3 Leading Edge

Figure 5. Typical distributions of metal temperature for LMF5 test section tubes.

Table 4. Average Tube Metal Temperatures at Measurement Locations (°F).

Test Section 1

Elevation	Tubes 1 and 8		Tubes 2 and 7		Tubes 3 and 6		Tubes 4 and 5	
	Pass 1	Pass 2						
21"	1106	794	1175	804	1361	829	1413	835
33"	1132	822	1204	838	1396	881	1450	892
45"	1132	850	1202	873	1390	933	1444	949
57"	1103	879	1202	908	1355	985	1393	1006
69"	1047	904	1104	940	1258	1033	1299	1059
81"	963	913	1009	952	1129	1055	1162	1084
93"	874	896	912	934	1001	1036	1021	1064

Test Section 2

Elevation	Tubes 1 and 8		Tubes 2 and 7		Tubes 3 and 6		Tubes 4 and 5	
	Pass 1	Pass 2						
21"	1211	908	1221	912	1233	916	1240	919
33"	1199	919	1210	921	1222	923	1230	925
45"	1184	933	1195	934	1209	937	1217	938
57"	1174	948	1180	951	1188	956	1194	958
69"	1123	965	1138	972	1157	980	1168	985
81"	1082	984	1099	994	1119	1007	1131	1014
93"	1047	1005	1064	1019	1084	1036	1095	1045

Test Section 3

Elevation	Tubes 1 and 8		Tubes 2 and 7		Tubes 3 and 6		Tubes 4 and 5	
	Pass 1	Pass 2						
21"	1101	909	1101	909	1101	909	1101	909
33"	1093	909	1094	909	1095	909	1095	909
45"	1026	911	1026	911	1026	911	1026	911
57"	1007	924	1008	924	1008	924	1009	923
69"	1003	961	1006	961	1008	962	1012	962
81"	1005	983	1005	984	1005	984	1005	984
93"	991	987	991	987	991	987	991	987

Test Section 3 (cont.)

Elevation	Tubes 1 and 8		Tubes 2 and 7		Tubes 3 and 6		Tubes 4 and 5	
	Pass 3	Pass 4						
21"	900	668	901	668	901	668	901	668
33"	883	671	883	671	883	671	883	671
45"	878	670	878	673	878	674	878	676
57"	877	643	877	663	877	669	877	712
69"	868	674	868	674	868	674	868	674
81"	869	698	870	698	870	698	870	698
93"	867	789	868	790	868	791	868	791

Measurement of Corrosion Scale Thickness and Internal Penetration Depth

The outer surfaces of polished tube cross-sections were examined with a microscopic image analysis system for measurement of corrosion scale thickness and internal penetration depth. Effective scale thickness was measured by microscopically scanning the surface to find the location visually appearing to have the thickest or most area of scale, capturing a frame at that location, summing all image pixel areas in that frame identifiable as scale, and dividing by the length of the surface in the image. Internal penetration was measured as the maximum depth anywhere along the surface (usually but not necessarily within the same frame from which scale thickness was determined) to which either intergranular or transgranular oxides or sulfides extended into the metal beyond the local scale.

Scale Morphology Evaluation

In addition to the quantitative measurements of wall thinning, scaling, and penetration, qualitative evaluations were made from polished sections of the morphological character of scales, internal penetration, and scale-deposit interaction. Notations were also made of the condition of the steam-side surface. It was intended to compare the gas-side scaling to that at the steam-side on the assumption that conditions at the steam-side would be relatively innocuous and good scale development would occur in the absence of deposits. However, steam-side attack was often found to equal or exceed that at the gas-side, probably as a result of the high oxygen content of the steam.

RESULTS

Results of evaluations performed on TS1 and TS2 tubes are presented below. Corrosion evaluations for TS3 tubes are as yet incomplete and will be reported subsequently as an addendum to this report.

Scaling and Penetration

All data from measurement of corrosion scale thickness and penetration depth on TS1 and TS2 tubes are given in Figure 6. The white portion of stacked bars represents scale thickness and the shaded portion represents penetration. The two are stacked since, together, they provide a

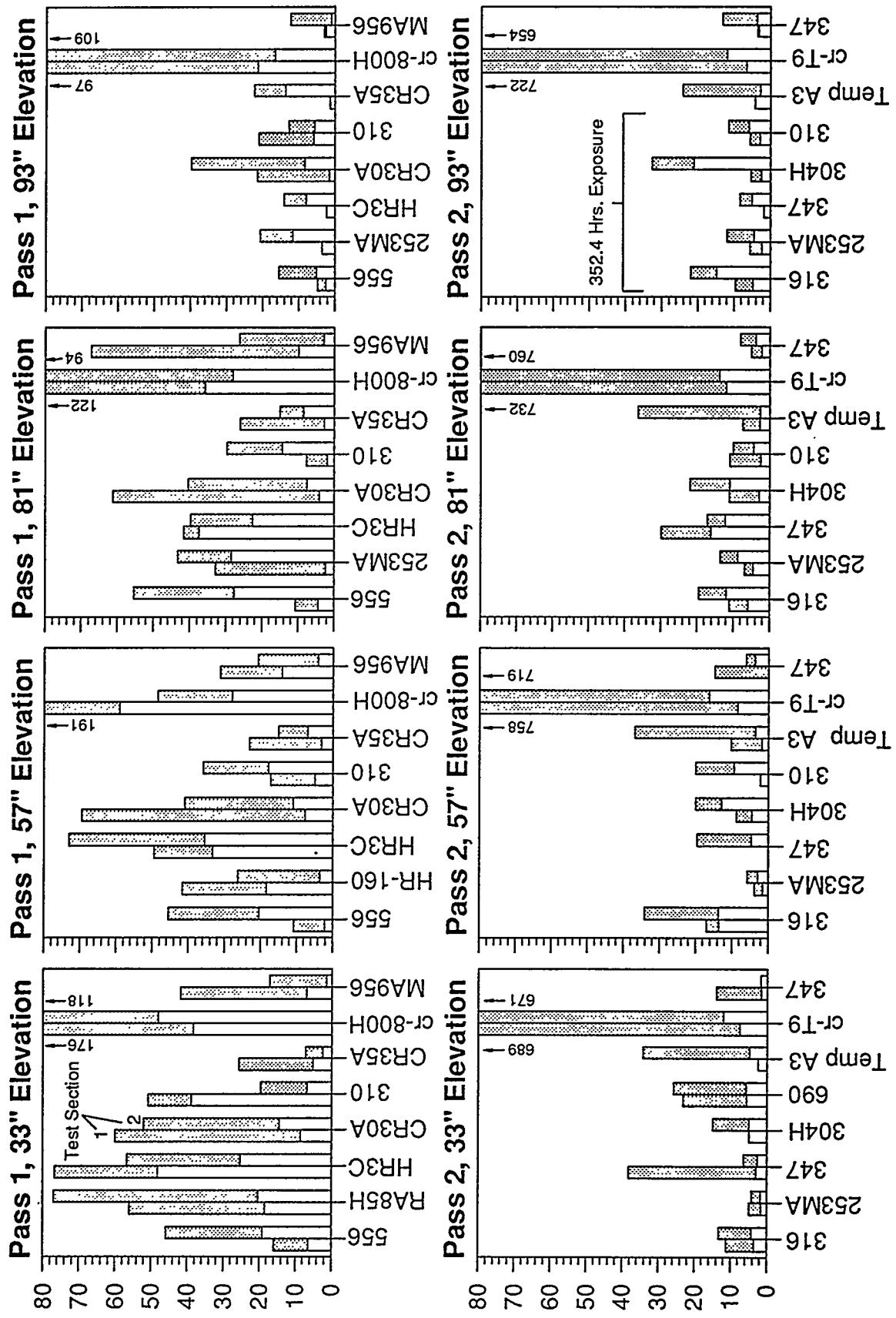


Figure 6. Corrosion scale thickness and penetration depth (in micrometers) for CFF superheater/ITAH tubes exposed to 991 test hours (except as noted) under LMF5 conditions.

measure of the total extent to which the external tube surface has been affected by the exposure environment. This measure is most useful for comparing the performance of the various tested alloys to each other or for comparing effects at various positions along a tube. Use as an absolute measure of corrosion rate or equivalent wall loss rate is not recommended for three reasons: the non-equality of scale thickness and metal consumption, unaccounted for metal loss due to migration into deposit and due to spalling, and the relatively very short exposure duration of the 1000 hours of test. Of the two bars in each bar group of the plot, the left one is for TS1 and the right one for TS2. The order of bar groups along the plot axis was the order of placement of alloys as tubes in the test module.

Looking at the more highly alloyed tube materials at the higher exposure temperatures of Pass 1, nickel-base alloy CR35A with 35% chromium is seen to be the best performer, while chromized alloy 800H was by far the worst. A statistical ranking of scaling and penetration performance of Pass 1 alloys in TS1 and TS2 was as follows from best to worst: CR35A, 310, 556, MA956, 253MA, HR3C, HR-160, CR30A, RA85H, and cr-800H. As a result of much scatter in the small data sample, however, the ranking may not necessarily represent the population. The ranking indicates the importance of both high chromium content and high chromium to nickel ratio. The low Cr:Ni ratio of CR35A is overcome by the high Cr content. Alloy 310 with moderate Cr content compared to CR35A performed nearly as well due to its high Cr:Ni ratio. Alloy MA956, with no nickel, did rather well with only 20% chromium, as did alloy 253MA with 21% Cr. A high chromium content is necessary to overcome nickel's susceptibility to sulfidation. Alloy HR3C is a variation of 310 with Nb, and should have as good or better performance. Its greater scaling and penetration in these tests was attributed to higher metal temperatures resulting from lower steam flow velocity through the larger tube. The chromizing treatment to alloy 800H, intended to raise its surface chromium content and Cr:Ni ratio, was clearly ineffective. The effect of higher tube temperatures with distance upward along Pass 1 is clearly shown by increasing scaling and penetration. Differences between data for TS1 and TS2 appear, however, to represent random scatter. Gas temperatures at TS1 were 500-600 degrees higher than at TS2 and deposits were accordingly much thicker and more sintered. It may be concluded that the corrosion mechanisms were dependent on metal and deposit temperatures but had little or no dependence on gas

temperatures or the thickness, hardness, density, temperature, or other characteristics of deposits remote from the tube/deposit interface.

The tube metals of Pass 2 of TS1 and TS2 were mostly less highly alloyed than those of Pass 1 due to the lower exposure temperatures there. The extent of scaling and penetration was rather low except for chromized alloy T9, for which penetration was very deep although scaling was low. Little or no difference was indicated along the length of Pass 2 or between Pass 2 and the 93" elevation of Pass 1, indicating a threshold in tube temperature at about 1200°F, above which corrosion increased much more rapidly. The performance ranking from best to worst was: 253MA, 310, 304H, 347, 316, Temp A3, 690, chromized T9, based on average scaling + penetration, as shown in Figure 7. Magnitudes of scaling and penetration were similar for alloys other than Temp A3, 690 and chromized T9. Internal penetration predominates when the inward anion diffusion rate greatly exceeds the outward cation rate.

Scaling and Penetration vs. Metal Temperature

Scale thicknesses measured for TS1 and TS2 tube samples are plotted against average metal temperature in Figures 8 and 9, while penetration depths versus temperature are shown in Figures 10 and 11. With only one data point for each alloy at a given temperature (i.e. location) and a large

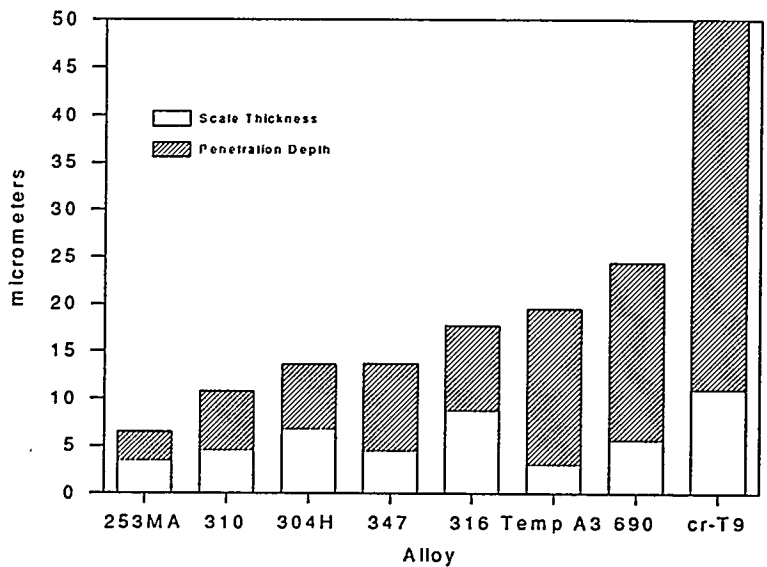


Figure 7. Average scale thickness and penetration depth for alloys in Pass 2 of TS1 and TS2.

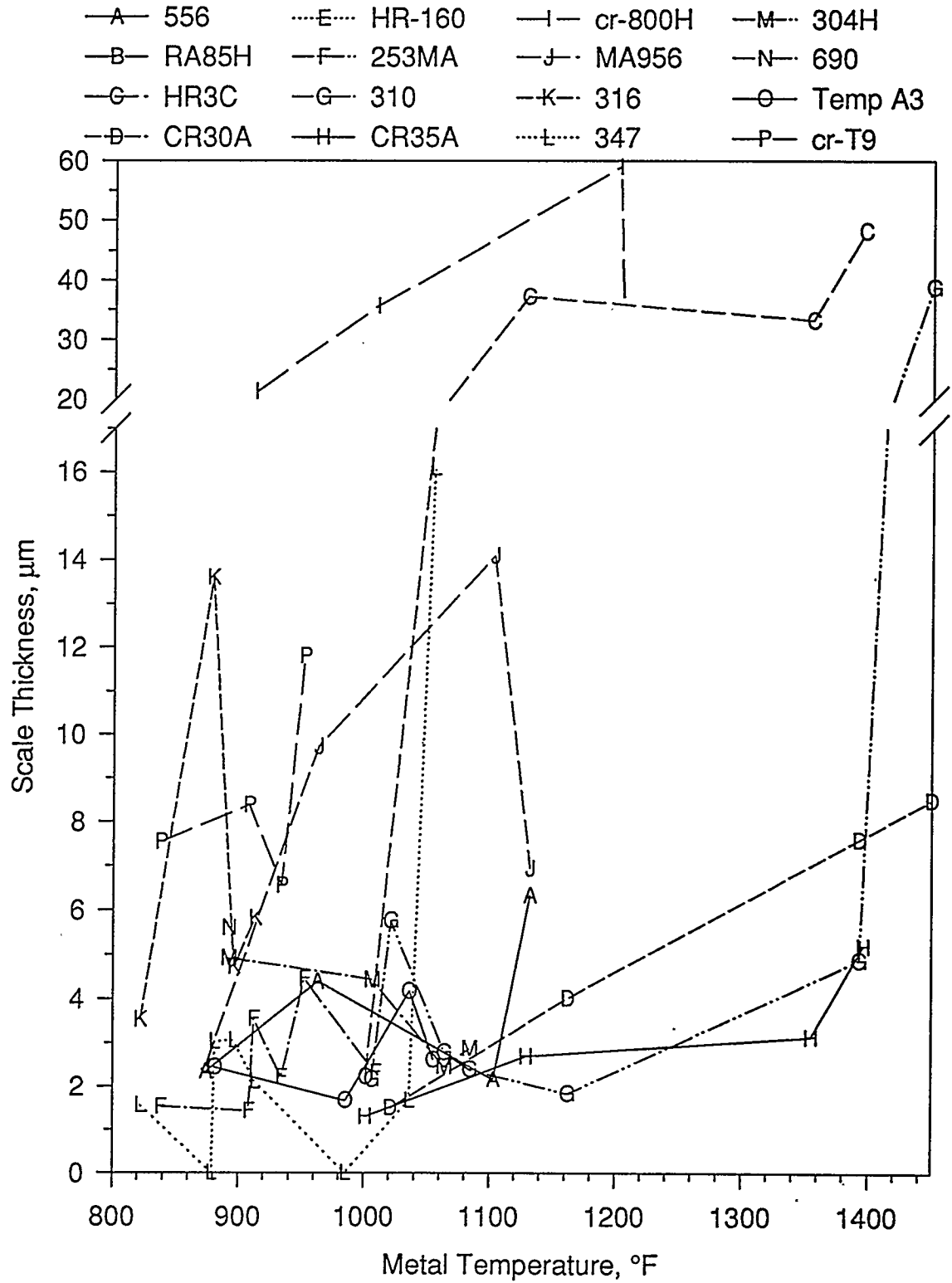


Figure 8. Scale thickness for TS1 alloys as a function of average exposure temperature.

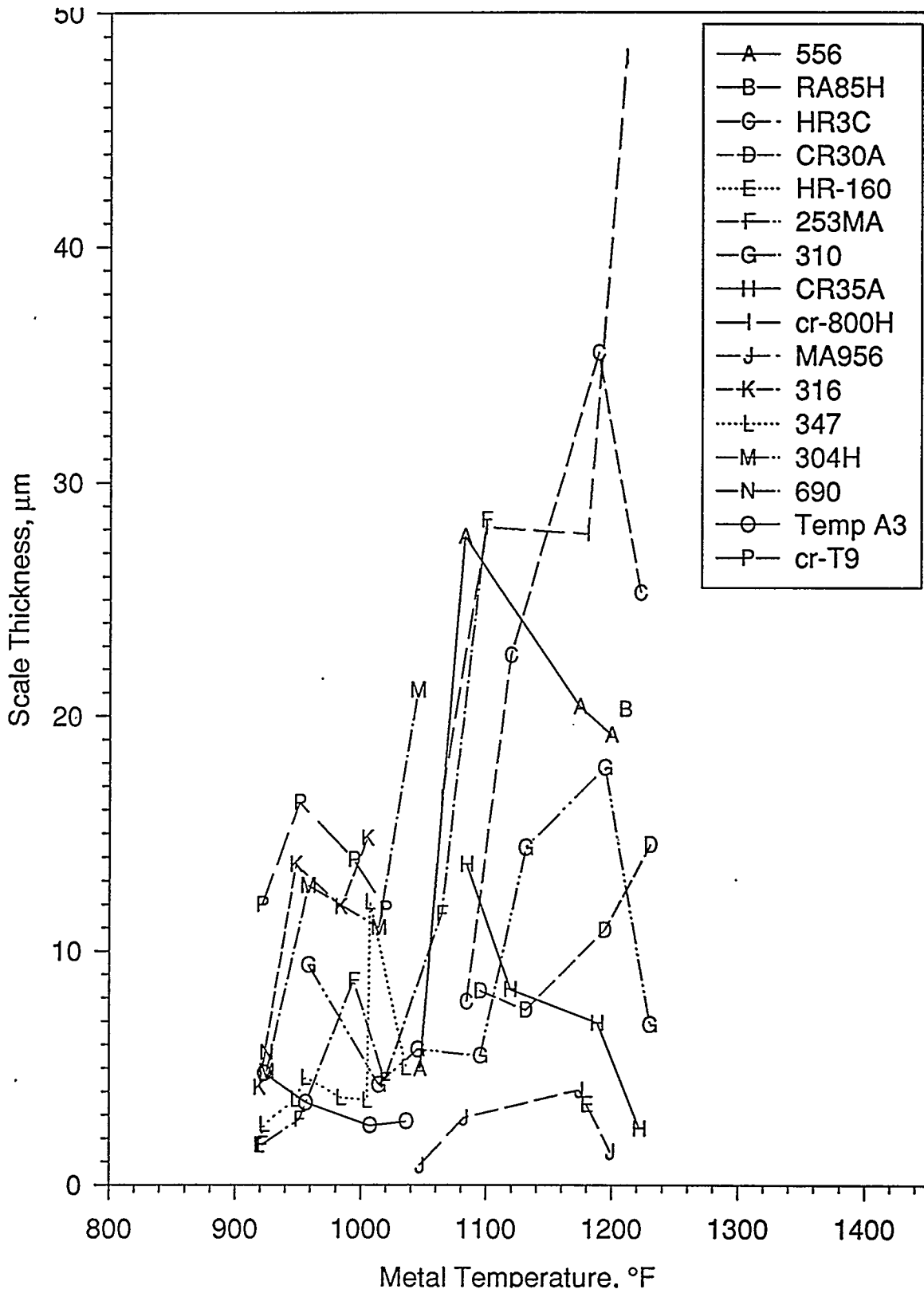


Figure 9. Scale thickness for TS2 alloys as a function of average metal temperature.

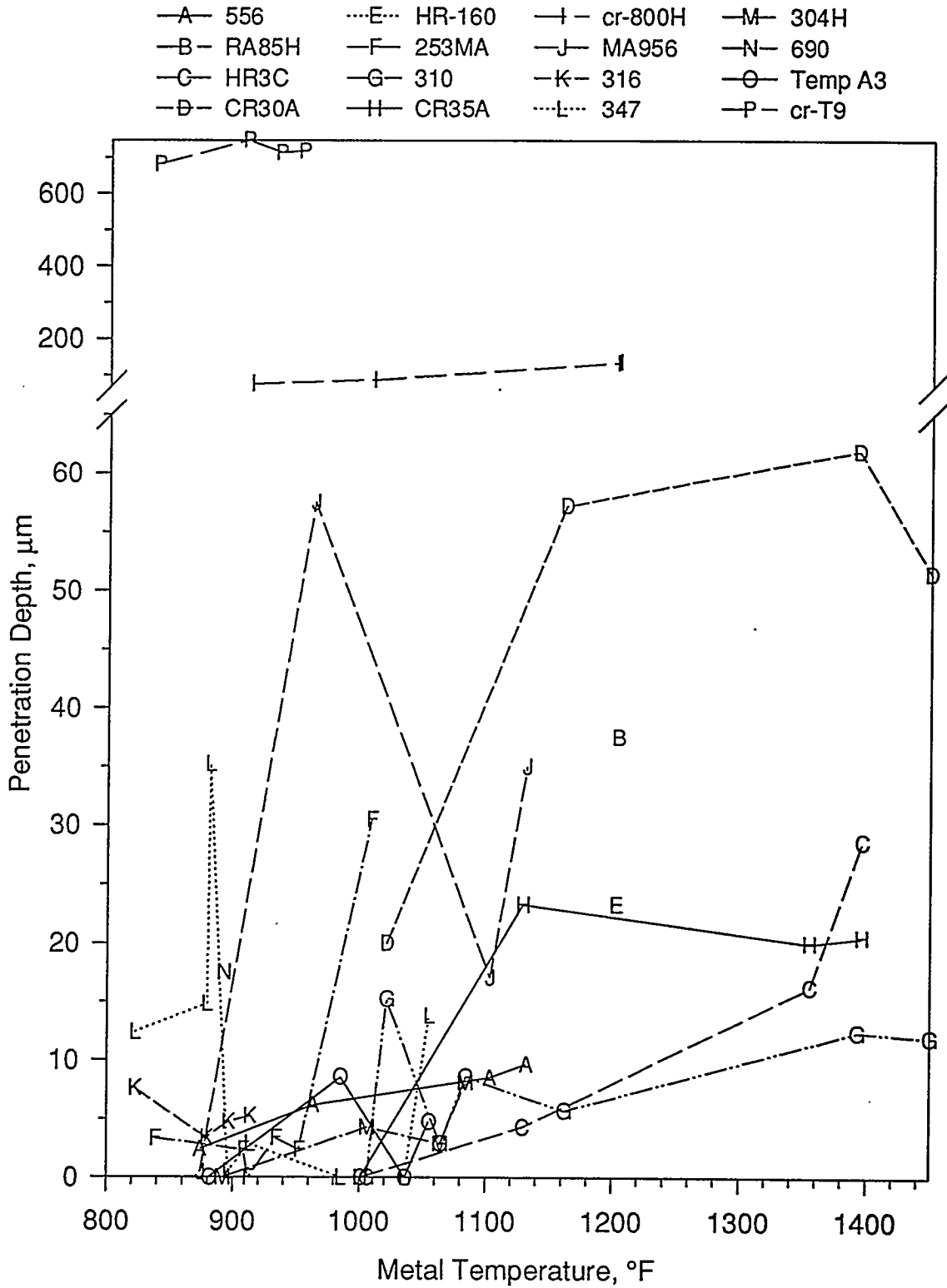


Figure 10. Penetration depth for TS1 alloys as a function of average metal temperature.

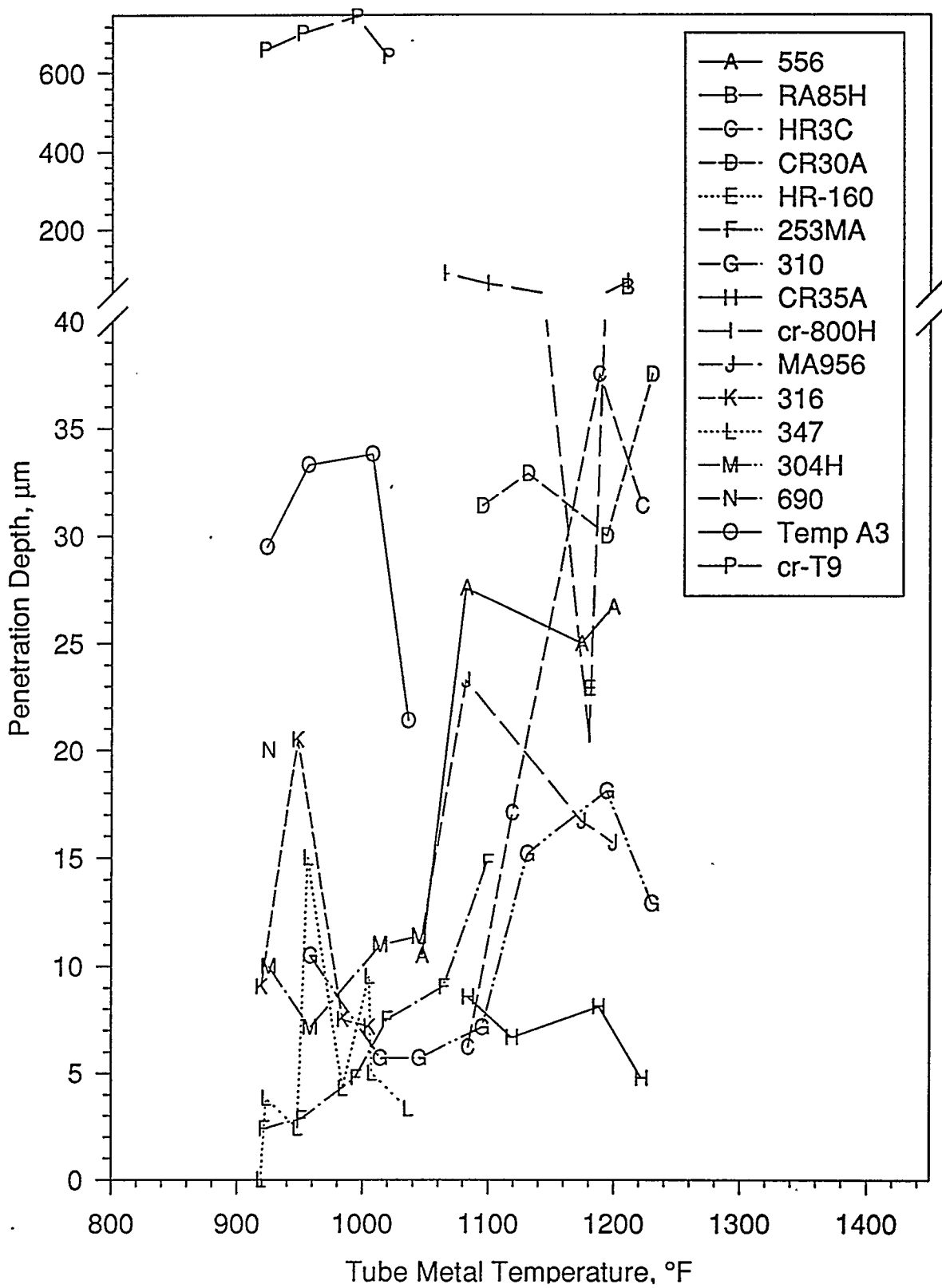


Figure 11. Penetration depth for TS2 as a function of average exposure temperature.

amount of inherent variability, it is only possible to draw conclusions as broad generalities. Namely, there seemed, in most cases, to be a trend of increasing alloy corrosion in terms of scale thickness and internal penetration with increasing tube metal temperature. For scaling, the temperature effect at TS2 appeared to be more marked than at TS1. However, CR35A at TS2 was a good example of a high chromium alloy for which corrosion decreased with temperature as a result of better, more protective scale formation. Several other high chromium alloys including 310, MA956, 556, and HR3C also showed decreased corrosion at the highest metal temperature.

Scale and Penetration Morphology Description

Views of the tube surface interfacial region showing the general morphological character of corrosion scales, subsurface oxide/sulfide penetration, and tube metal oxide precipitate dispersal in the deposit are given in Figures 12, 13, 14, and 15 for TS1 pass 1, TS2 pass 1, TS1 pass 2, and TS2 pass 2, respectively. These views are in the region of the highest metal temperature for each alloy. With the exception of the cr-800H and cr-T9 alloys, which were much more severely attacked than other alloys, the views were all at the same magnification. Differences in the depicted extent or character of corrosion for particular alloys between TS1 and TS2 are less indicative of real differences in average or overall corrosion at the two locations than of the random variability which is typical of such corrosion. Superior performance was exhibited at the higher metal temperatures of pass 1 by alloys CR35A, MA956, 310, 556, and HR-160. At pass 2, alloys 253MA and 347 did well, alloys 304H, Temp A3, and 316 less well, alloy 690 poorly, and alloy cr-T9 very badly.

CR35A - Typical of many highly heat resistant alloys, the performance of CR35A improved dramatically with rising temperature (within a certain temperature range), the reverse of what might generally be expected, owing to the more uniform, higher chromia, and hence more protective scale formed at the higher temperatures. At the upper and hotter end of pass 1, CR35A exhibited very thin scale, hardly any penetration, and essentially no diffusion zone of metal (red or darkened zone variably with metal oxide precipitates outwardly adjacent to the normal scale) into the tube deposit. Performance deteriorated with distance down pass 1 toward the cooler end, however, where there was in general a two layer scale, both porous, with the outer in various degrees of dispersal into the deposit. There the diffusion zone was typically 40 μm thick, with metal oxide precipitates dispersed

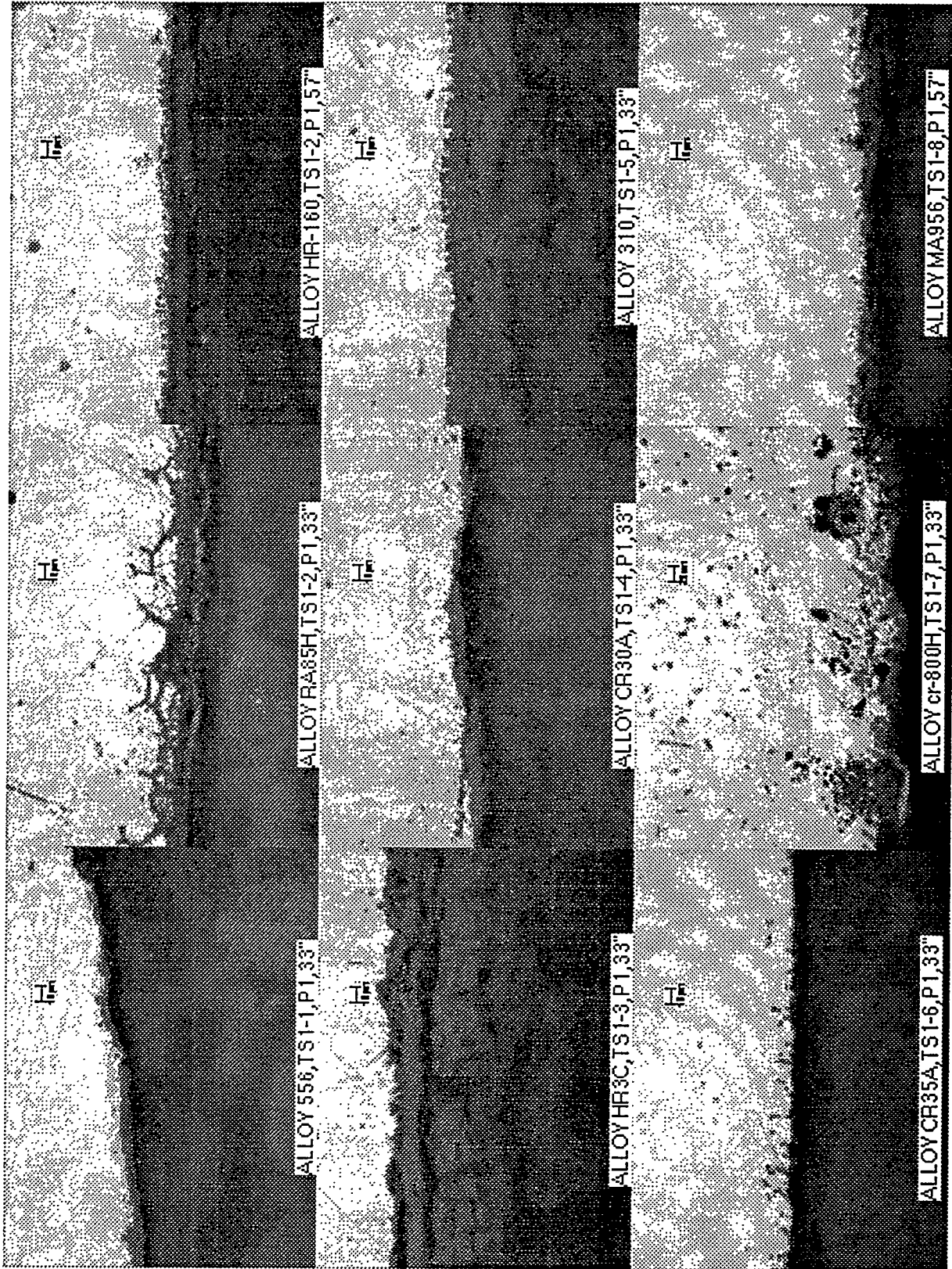


Figure 12. Scale and penetration morphology for alloys of TSI pass 1.

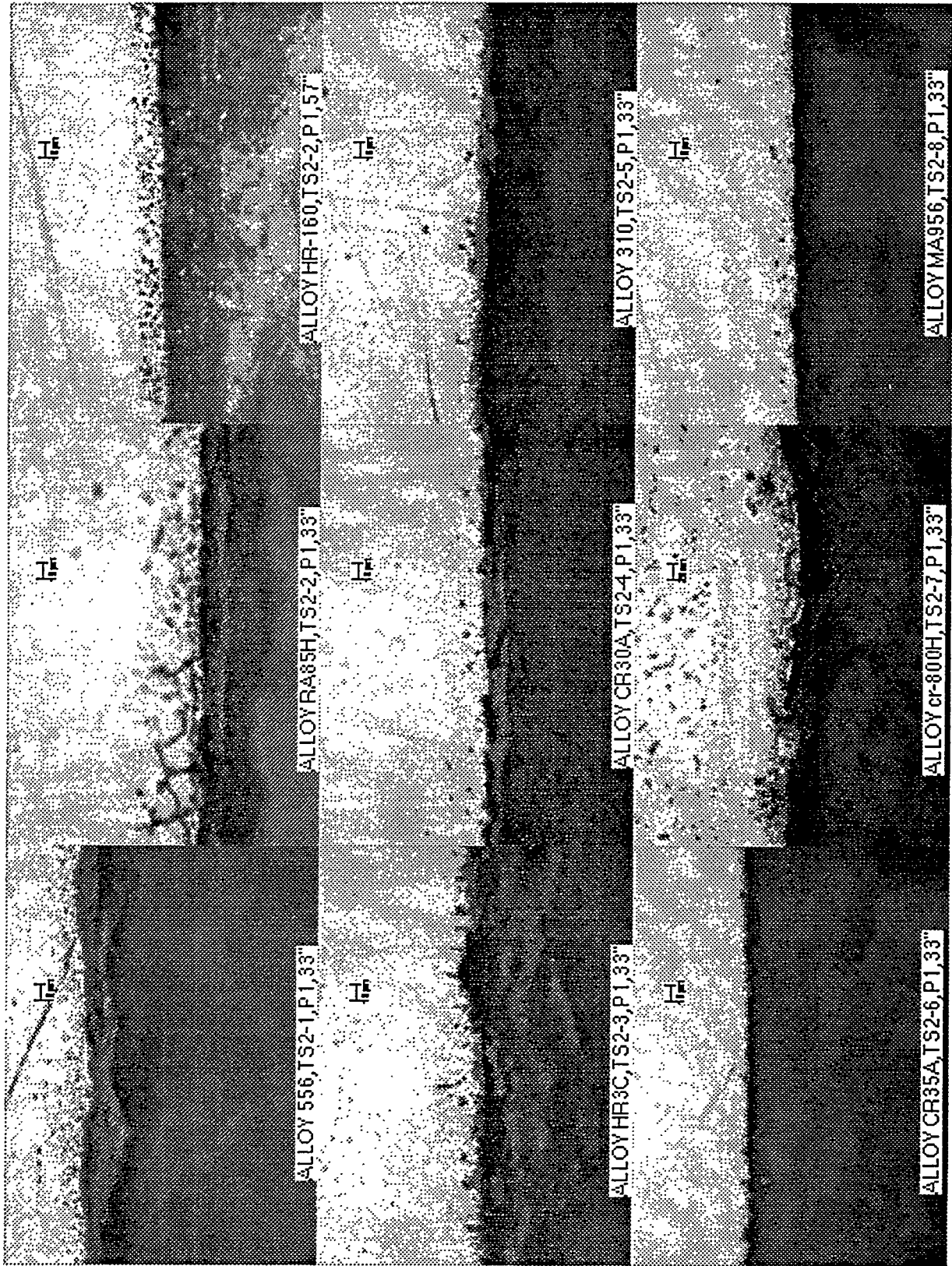


Figure 13. Scale and penetration morphology for alloys of TS2 pass 1.

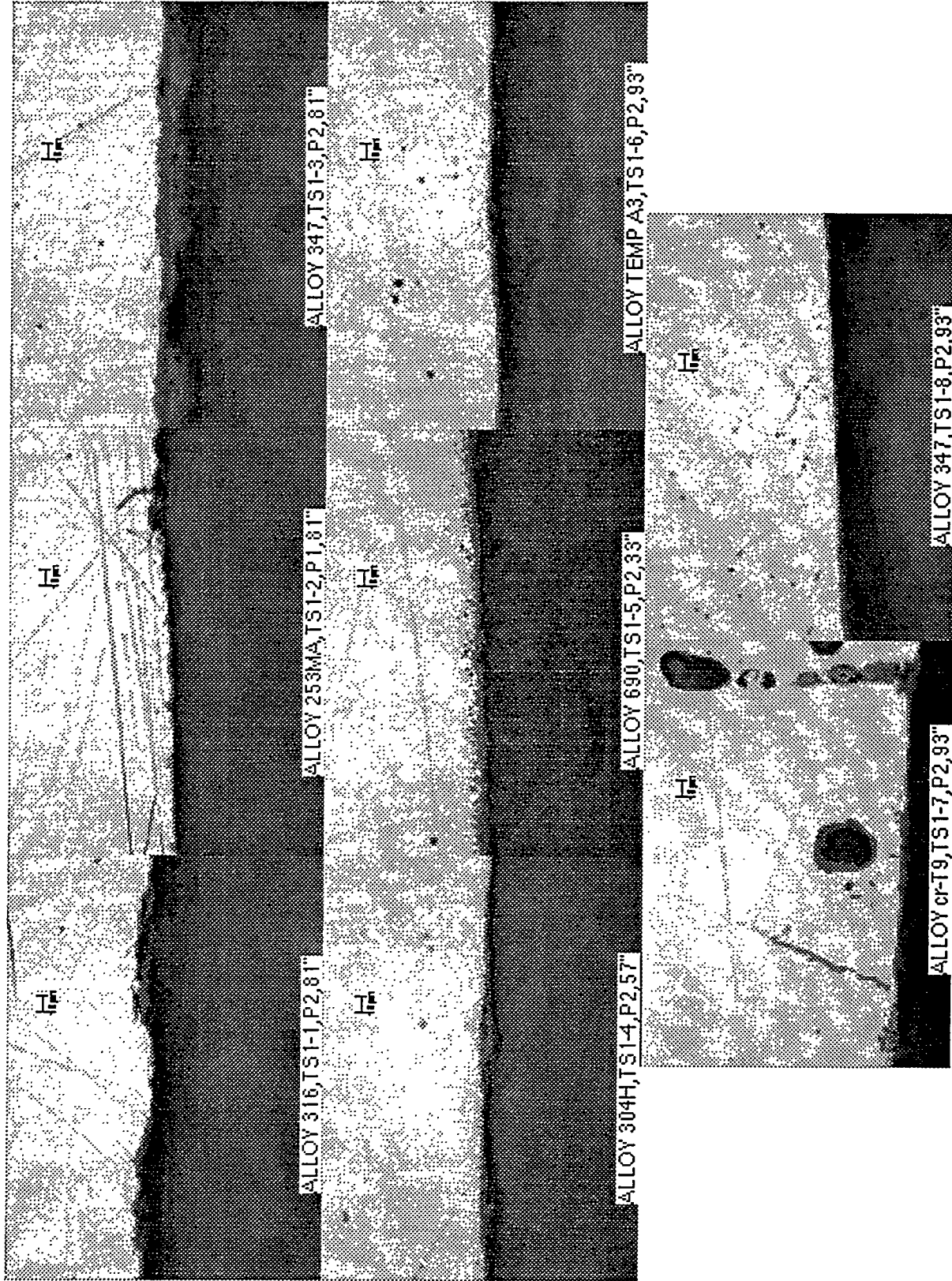


Figure 14. Scale and penetration morphologies for alloys of TS1 pass 2.

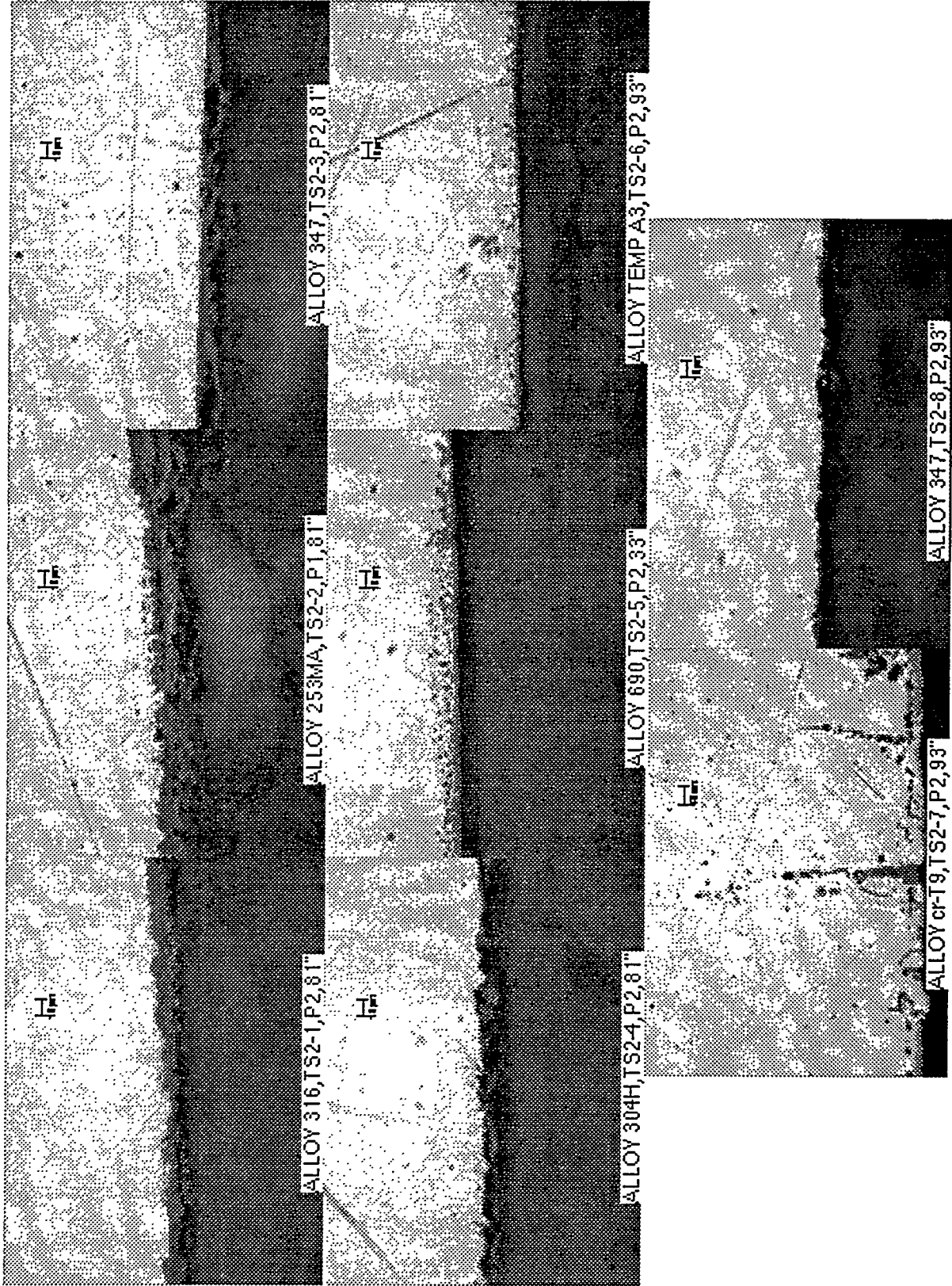


Figure 15. Scale and penetration morphologies for alloys of TS2 pass 2.

within it. In some instances, there was no normal scale at the interface, only the dispersed oxides. Subsurface penetration was very shallow and transgranular.

MA956 - Much of the surface possessed only an extremely thin (<5 μm) scale film, transgranular penetration only about 15 μm deep, and little or no diffusion zone in the deposit. Other areas had a little thicker (~15 μm) scale, deeper penetration (up to 35 μm), and a diffusion zone about double the scale thickness, containing a small amount of oxide precipitates. There was one area on one sample which possessed some broad, rather shallow, pitting. Much deeper and more extensive pitting was seen at the steamside. Both were possibly caused by downtime aqueous corrosion under conditions absent in actual service.

310 - At cooler locations (pass 2 and the bottom of pass 1), the scale layer on alloy 310 was very thin (<5 μm). At the hottest locations, scale thickness was variable ranging from hardly any to about 40 μm thick, as in Figure 12. That scale appeared porous and contained islands of the same red salt phase seen outward of the scale in the deposit diffusion zone. Some regions revealed a two layer scale, the inner being inward growing and the outer being outward growing, with often a gap between them. Penetration was shallow (up to 18 μm) and transgranular, with what appeared to be very fine sulfide precipitates inward of the oxide precipitates.

HR-160 - Corrosion scale thickness varied from zero to about 40 μm . Two layers were present, an inner darker grey inward growing layer and an outer lighter grey outward growing layer. There was a variable amount of metal oxide of the same appearance as the outer scale layer precipitated in the brown, darkened layer of what was originally deposit adjacent to the tube. As precipitation proceeded with exposure time, the spaces between individual particulates were filled in and areas initially containing the particulates would be joined to and would constitute part of the outer scale layer. Since this alloy is nickel based with 27% cobalt substituted for iron, the diffusion layer in the deposit lacked the red coloration associated with high iron containing alloys. Sulfide precipitates were observed within the inner scale layer and between the two layers. Internal penetration existed as fairly shallow (up to 25 μm) transgranular precipitates or protrusions of the inner scale, being the mode of growth of the inner scale layer.

556 - The character of scale and penetration was much the same as for HR-160 and performance in terms of extent of scaling and penetration were also similar. Corrosion was more at TS2 than at TS1.

CR30A - Alloy CR30A exhibited fairly thin (<15µm) scales similar to those of alloy 310. However, despite its higher (30%) chromium content, penetration was much deeper (20-60 µm). This is attributable to its lower chromium to nickel ratio. Much of the penetration consisted of a distribution of fine, light grey transgranular sulfide particulates. Also, there were larger transgranular oxide precipitates and infrequent deep intergranular oxide penetration.

HR3C - While alloy HR3C is a variation of 310 with Nb, Ta, and N additions, and would be expected to have as good or better ash corrosion performance, that was not the case of the tested HR3C tubes. There was a two-layer, relatively thick (up to 50 µm) scale, increasing in thickness with increased temperature. There was the same inner inward growing layer and outer outward growing layer seen with other alloys, generally separated by a red salt filled parting. Both scale layers were very porous. In some places most of the outer layer was in fact a dense distribution of oxide precipitates in a matrix of red salt. The oxide precipitate density decreased with outward distance such that there was a red outer zone having only a little oxide. Even further out, the deposit was colored somewhat by cation diffusion from the tube. At TS2, the outer scale existed as multiple (up to five) layers. It appeared that successive outer scale layers grew by precipitation in the red salt adjacent to the inner scale layer and were spalled outward, with the vacated space being refilled with deposit which converted to the red salt. Internal penetration consisted of transgranular oxide and sulfide precipitates. As speculated earlier, the larger size (2.24" O.D.) of the HR3C tube undoubtedly resulted in higher metal temperatures (no temperature measurements were made on that tube), accounting for the more severe corrosion observed as compared to alloy 310.

RA85H - Alloy RA85H has silicon and aluminum additions and in isothermal gaseous oxidative service performs close to 310. It is particularly suitable for combined carburization and sulfidation service, as in waste incinerators. However, in ash corrosion, the silicon and aluminum additions appear to be considerably inferior to chromium. For RA85H (and also MA956 and

253MA) high temperatures beyond the usable range in ash corrosion service are required to optimize the protectiveness of scales augmented with silicon and or aluminum. While scale thickness (~20 μm) was not more than some of the much higher alloyed materials such as 310 or 556, internal intergranular penetration (40-60 μm) was the main problem. There were also transgranular oxides and sulfides.

cr-800H - Alloy 800H has a much too high nickel content for use in sulfidizing conditions such as ash corrosion. However, it has good creep rupture characteristics and steamside compatibility. A chromizing treatment was applied to evaluate the amount of improvement in gas-side compatibility. Chromizing was effective in that much of the surface was found to have negligible corrosion with only about a 5 μm thick scale and no penetration. However, owing evidently to nonuniformities in the chromized layer, other areas were severely attacked with quite deep pitting (20-60 μm) or broad localized surface recession plus extensive transgranular penetration (up to 200 μm) extending in some cases deeper than the chromized layer.

253MA - Scale thicknesses for alloy 253MA were considerably thicker at TS2 (28 μm max) than at TS1 (4 μm max), because TS1 metal temperatures were higher and the protectiveness of 253MA scales increases with temperature. As stated earlier, alloys such as 253MA which contain silicon, aluminum, or rare earth metals such as cerium for enhanced oxidation or high temperature corrosion protection are only able to form optimally protective scales at quite high temperatures, beyond the range of serviceability in ash corrosion. In fact, in isothermal oxidation, the microalloy beneficial effects for 253MA are most pronounced at around 2000°F.³ As a result, TS1 scales were thin and uniform with little internal penetration present, while those at TS2 were thicker, nonuniform, and porous and outward of the scale was a red salt layer of variable thickness and variable metal oxide content. Penetration at TS2 consisted of shallow transgranular oxides.

Temp A3 - Tempalloy A3 is a higher chromium analog of 347, plus nitrogen strengthening. Scales were thin (<5 μm). But again, TS2 penetration was more (20-30 μm) than at TS1 (<10 μm), because the temperatures at TS2 were lower and the scales there were not as protective, being porous and discontinuous. TS2 penetration consisted of intergranular and transgranular oxides. On

the deposit side, a red diffusion zone about double the scale thickness existed, containing a dispersion of metal oxides.

690 - The placement of alloy 690 was at the cool end of pass 2, which was likely too cold for proper scale development for this high chromium, nickel base alloy. While uniform, continuous scales existed, they were thicker (~6 μm) at this location than for alloys such as 347, and transgranular oxide and sulfide penetration was as much as 20 μm deep. Nickel base alloys, being susceptible to sulfidation, must form well developed, high chromia scales for protection, which for alloy 690 with 29% chromium is possible at high temperatures but not at low temperatures.

347 - Two layer scales were observed, the inner inward growing and the outer outward growing. The outer scale had grown by metal oxide precipitation in the red salt zone which was originally deposit and had enclosed ash spheres and splotches of red salt. Outward of the scale was red salt containing scattered oxide precipitates. Scale and penetration morphology was variable in that in many areas the scale was thin ($\leq 3 \mu\text{m}$), uniform and continuous with little or no penetration, while in other areas the scale was of irregular thickness (up to 16 μm), sometimes highly disorganized and fragmented, and with attendant deeper internal penetration (to 40 μm) and outward metal diffusion to the deposit.

304H - Behavior of alloy 304H was similar to alloy 347, except that in all cases alloy 304H did considerably worse at TS2. At TS1 scales were thin and continuous and penetration was only very shallow intergranular oxides. At TS2 scales were thicker, less compact, more porous, resulting in deeper penetration and outward metal diffusion.

316 - Of the three 18-8 stainless steel grades tested, alloy 316 did least well, as would be expected from its somewhat lower chromium content. Also, Mo is detrimental in high temperature ash corrosion. The same sort of morphologies were observed as for the other 18-8's. In areas where scales were smooth and continuous, only transgranular penetration was observed, while intergranular penetration accompanied the occurrence of irregular, nonuniform scales.

cr-T9 - Scales on the chromized alloy T9 tubes were thin ($\leq 16 \mu\text{m}$), being no thicker than for the other alloys tested, showing the effectiveness of chromizing in that regard. However, penetration was very deep, in excess of $700 \mu\text{m}$. This penetration occurred at rare, isolated locations, evidently at defects in the chromized layer and took the form of transgranular, linear cracking approximately perpendicular to the surface. Thus, protection of alloys which have wholly inadequate resistance to ash corrosion by chromizing was shown to be infeasible. If the base alloy itself had reasonably adequate resistance, a considerable performance improvement, particularly in regard to scaling, can be achieved by chromizing at a relatively low cost. However, isolated occurrences of attack can be expected of the same modes as the unchromized alloy, the most severe of which would approach the level of severity experienced by the unchromized alloy.

Wall Thinning Data

Figures 16 and 17 present data on tube wall thinning as derived from pre-exposure ultrasonic wall thickness measurements and post-exposure wall thickness measurements using either microscopy with cut and polished sections or a micrometer. As pointed out earlier, there was a considerable potential for error in these measurements, arising partially from the difficulty of making before and after measurements at the same locations, and partially due to the inadequate precision of wall thickness measurements, particularly by ultrasonics, to correctly indicate the minute amount of surface recession occurring during the short exposure. Also, for the micrometer method, there was a potential for either incomplete scale removal or base metal loss in the glass bead blasting operation, as well as an ignored amount of scaling on the steam side.

However, the relative behavior of the wall recession data with respect to the various alloys was in quite reasonable agreement with microscopic scale measurement results. The two chromized alloys showed high losses compared to the others. Alloy 316 showed considerably higher loss than 304H and 347. Alloy HR3C showed an increase with temperature while 310 showed a decrease, in agreement with microscopic results. Large scatter for alloy 253MA data was also in keeping with other observation, as explained by the alloy's inability to form a highly protective scale at the lower temperatures. Again, alloy CR35A seemed to be the best performer. It must be remembered that

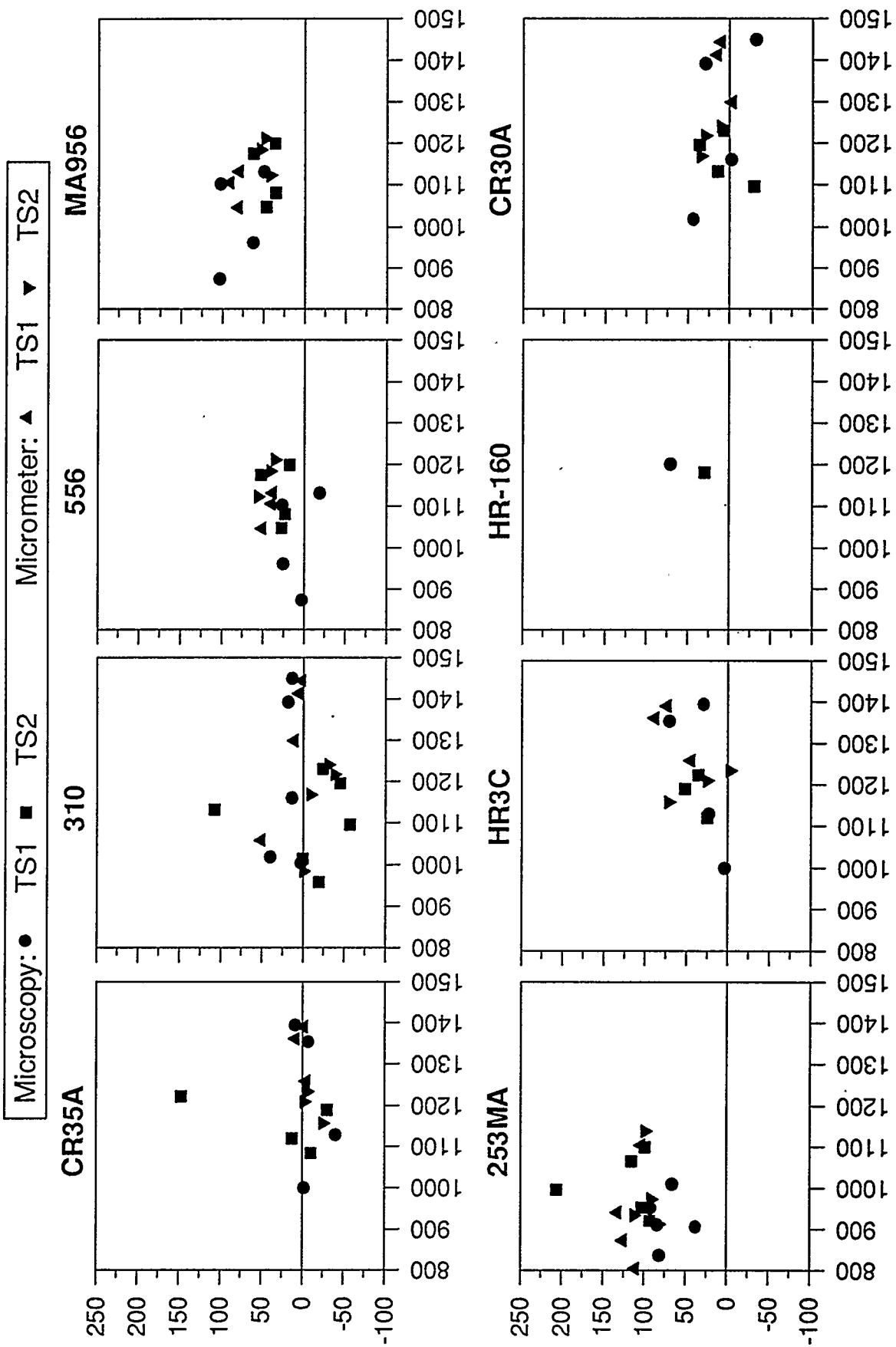


Figure 16. Fireside tube surface recession (micrometers) (averaged at a given cross-section) plotted against average metal exposure temperature (°F).

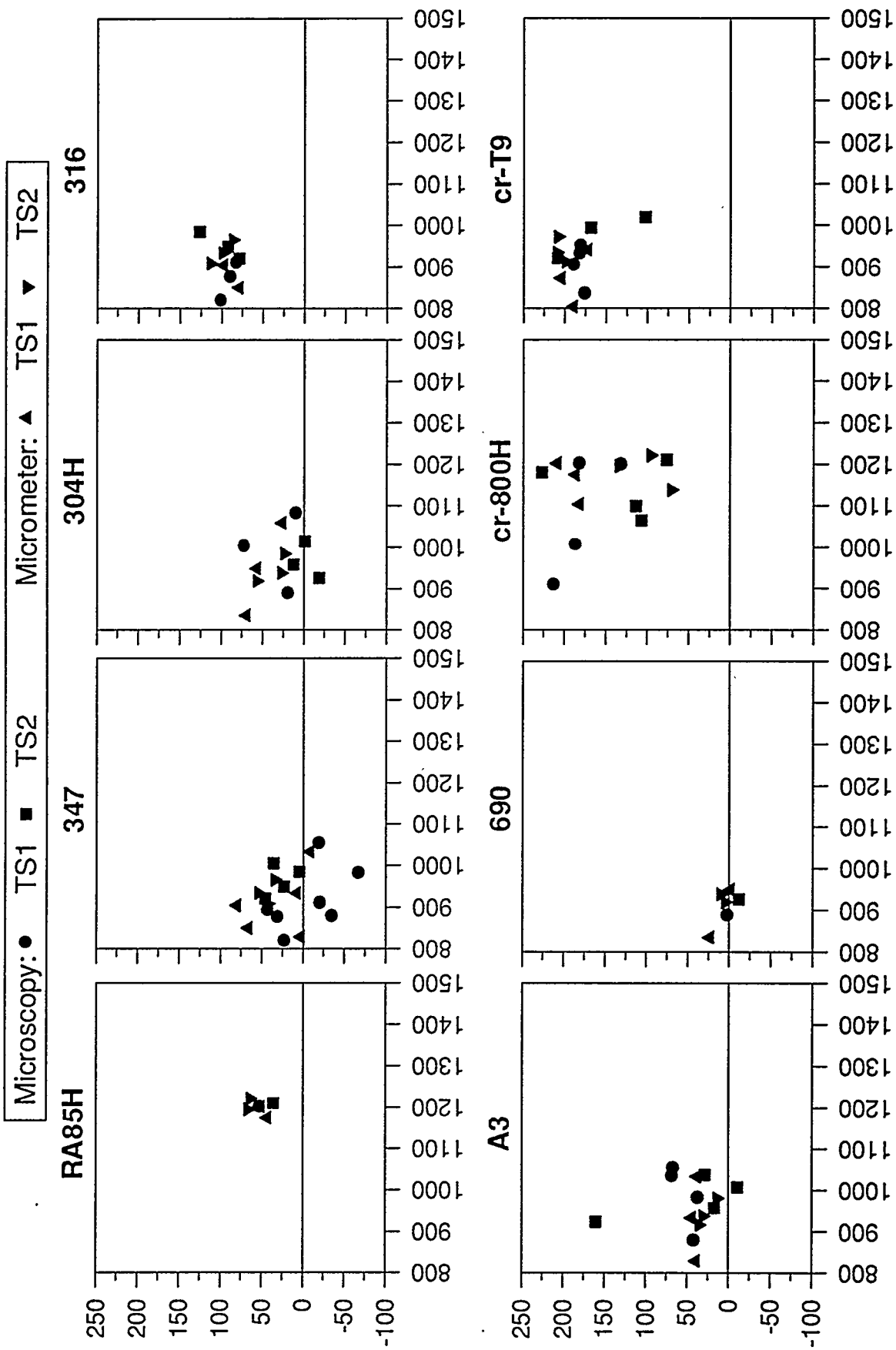


Figure 17. More fireside tube recession (micrometers) (averaged at a given cross-section) plotted against average metal exposure temperature (°F).

internal penetration is not accounted for in these measurements. Thus, while alloy CR30A wall recession data looked very good, microscopic examination revealed deep penetration.

DISCUSSION

Behavior of alloys subjected to corrosion by deposits of MHD ash containing potassium sulfate as the major component exhibit some characteristics in common with conventional coal ash corrosion in an oxidizing flue gas,⁴ in which case potassium sulfate is a minor constituent in the bulk deposit but is concentrated adjacent to the tube surface where it becomes the major constituent. These similarities include the following:

1. With respect to alloy composition, chromium content exerts a dominant influence on corrosion resistance, arising from the very low rates of ionic diffusion through chromium oxide scales and films.
2. In addition to chromium content, other alloying elements, temperature, and thermal cycling affect the ability of an alloy to form and maintain a protective oxide surface scale.
3. Solid state corrosion occurs by an oxidation/sulfidation mechanism, in which oxides vastly predominate as reaction products, but the presence of sulfur accelerates oxidation and allows sulfidation by making the oxide formed less protective.
4. High nickel content has a detrimental effect owing to nickel's tendency to sulfidize and the potential for formation of a nickel sulfide low melting eutectic able to catastrophically flux oxide scales.
5. Surface scale types and morphologies are generally the same.
6. For austenitic alloys, internal penetration is generally present and is often the principal factor in effective wall loss.
7. Outward migration of metal ions into the deposit occurs, with subsequent precipitation of metal oxides dispersed in the deposit.

A major difference, however, between MHD and conventional coal ash corrosion is the absence in the MHD case of liquid phase attack by complex alkali iron (or aluminum) trisulfates. Occurrence of these phases in the conventional coal ash case causes catastrophic corrosion above the molten range of approximately 1100-1400°F by fluxing of protective oxide scales from heat exchange tube

surfaces. Their formation requires a normal alkali sulfate precursor adjacent to the tube surface and a sufficient level of SO_3 . In MHD with $K_2/S > 1$, tying of sulfur to potassium as $K_2\text{SO}_4$ prevents high SO_3 levels. While prevention of liquid phase attack in conventional coal-fired power plants has required limiting steam temperatures to about 1050°F , or burning only select low alkali, low sulfur coals, or coal cleaning, MHD opens the door to operating steam and air heating tubes at substantially higher temperatures and realizing the attendant substantial improvement in overall conversion efficiency.

A comparison between corrosion with the Montana Rosebud coal during the LMF5 test series with that occurring with Illinois #6 coal during the prior LMF4 test series is made by calculating corrosion rates assuming some rate behavior. Table 5 gives average linear and parabolic corrosion rates based on the sum of scale thickness and penetration depth for the four alloys used in both LMF4 and LMF5. (LMF4 data with three exposure durations shows that actual corrosion kinetics appears to be closer to parabolic rather than linear.) For each alloy, all measurements made on a given tube pass are averaged since there was only a weak dependence on metal temperature over each pass and little or no dependence on angular position around the tube. In general, considerably less corrosion is indicated for the Montana Rosebud coal than for the Illinois #6 coal. This agrees with qualitative observations of scaling and penetration. The most likely cause for more severe corrosion with the Illinois #6 coal was its higher sulfur content ($\sim 3\%$ as opposed to $\sim 0.7\%$ for Montana Rosebud) resulting in a much higher K_2SO_4 content of the deposits ($\sim 75\%$ in the bulk deposit for Illinois #6 versus $\sim 35\%$ for Montana Rosebud). As discussed earlier, sulfur diffused into the oxide scale formed at the tube surface alters both the defect structure and the mechanical properties of the oxide, making it less protective against outward metal ion diffusion and inward oxygen and sulfur diffusion.

SUMMARY AND CONCLUSIONS

Iron-based and nickel-based alloys covering a broad compositional range were exposed for approximately 1000 hours to conditions simulative of fire-side superheater and intermediate

Table 5. Comparison of average corrosion rates (mm/yr) in LMF5 tests with Montana Rosebud coal to LMF4 tests with Illinois #6 coal.

a. Linear												
TS1						TS2						
Alloy	LMF4				LMF5		LMF4				LMF5	
	500 hrs.		1500 hr.		1000 hrs.		500 hrs.		1500 hrs.		1000 hrs.	
	Pass 1	Pass 2	Pass 1	Pass 1	Pass 1	Pass 2	Pass 1	Pass 2	Pass 1	Pass 1	Pass 1	Pass 2
316	1.02	0.32	0.97	0.49	-	0.12	1.41	1.02	1.09	-	-	0.20
304H	0.62	0.18	0.75	0.47	-	0.07	2.10	0.38	1.10	0.77	-	0.17
253MA	0.33	0.14	0.33	0.19	0.16	0.05	0.70	0.41	0.49	-	0.28	0.07
310	0.11	0.44	0.32	0.11	0.21	0.06	0.53	0.15	0.65	0.35	0.22	0.13

b. Parabolic												
TS1						TS2						
Alloy	LMF4				LMF5		LMF4				LMF5	
	500 hrs.		1500 hr.		1000 hrs.		500 hrs.		1500 hrs.		1000 hrs.	
	Pass 1	Pass 2	Pass 1	Pass 1	Pass 1	Pass 2	Pass 1	Pass 2	Pass 1	Pass 1	Pass 1	Pass 2
316	0.24	0.08	0.40	0.22	-	0.04	0.34	0.24	0.45	-	-	0.07
304H	0.15	0.04	0.31	0.23	-	0.02	0.50	0.09	0.46	0.37	-	0.06
253MA	0.08	0.03	0.14	0.09	0.05	0.02	0.17	0.10	0.20	-	0.10	0.02
310	0.03	0.03	0.13	0.05	0.07	0.02	0.13	0.04	0.27	0.17	0.07	0.04

temperature air heater service in MHD power generating plants burning a relatively low sulfur, high ash, and high volatile coal, Montana Rosebud. Tests were conducted in a 20 Mw_t facility with test alloys in the form of 7.5 feet long pendant u-shaped tubes mounted in three duct modules called test sections, located in regions of successively lower gas temperature of interest in simulating secondary superheater, reheater, primary superheater, and intermediate temperature air heater service. Steam cooling was used to maintain tube metal temperatures ranging from 700°F to 1400°F. Corrosion occurred beneath deposits containing approximately 35% potassium sulfate, 30% potassium carbonate, and 30% flyash. After exposure, corrosion of tube samples was evaluated in terms of scale thickness and depth of internal penetration, comparison of remaining wall thickness with initial ultrasonic thickness measurements, and qualitative microscopic evaluation of scale, penetration, and deposit morphologies. Post-test evaluations were not performed on Test Section 3 tubes because of overheating during exposure. The following conclusions were made from the evaluations performed on tubes from Test Sections 1 and 2, together with application of relevant observations and conclusions from prior work:

- 1. Corrosion resulted from solid state interaction of tube metals and their scales with K_2SO_4 in the deposits.**
- 2. Complex alkali trisulfates such as $K_2Fe(SO_4)_3$, responsible for potentially severe conventional coal ash corrosion, are not normally present in MHD as a result of low SO_2 and SO_3 concentrations in the flue gas.**
- 3. Many of the corrosion characteristics in these tests were similar to those occurring in liquid phase coal ash corrosion. These included having the same corrosion precursor (K_2SO_4), the same type of scales, and the same migration of iron into the deposit to produce $FeSO_4$, and precipitation of iron oxide near the outer boundary of the $FeSO_4$ as a result of decreasing sulfur partial pressure and increasing oxygen partial pressure.**

4. Corrosion resulted in oxide scales containing sulfur either in solution or as discrete sulfides. Sulfur penetration of the scale resulted in enhanced outward metal ion migration and production of Cr-Fe scales often having multiple layers. Much separation of these scale layers and scale fracturing occurred, augmented by the relative large number and intensity of thermal cycling which occurred. A red phase containing iron and sulfur, assumed to be FeSO_4 , between the scale and the deposit appeared to be a brittle phase prone to spalling and to contributing to scale spalling. This scale damage resulted in further corrosion, and this process could eventually reach a break-away stage wherein scales would no longer be repaired due to subsurface chromium depletion and rapid attack would occur. However, cyclic conditions were far more severe in these tests than would be expected in actual service.
5. Internal penetration of most of the austenitic stainless steels occurred as a result of inward migration of oxygen and sulfur being faster than the outward migration of cations. This penetration resulted in subscale sulfides in some cases, in transgranular oxidation/sulfidation of the surface grains, and intergranular penetration to a depth of several grains, depending upon the chromium content.
6. Resistance to corrosion generally increased with increasing alloy chromium content. Alloy CR35A with 35% Cr was the most resistant of those tested.
7. Monotonically increasing corrosion with temperature was not generally observed due to the the ability of high chromium alloys to produce more protective surface scales at high temperatures than at lower temperatures.
8. There was little difference in corrosion between TS1 with a gas temperature of around 2250°F and hard, thick deposits, and TS2, with a gas temperature of about 1700°F and

friable deposits. There was, however, evidence of more scale spalling at the higher gas temperature.

9. There was little dependence of corrosion on angular position around the tube. Higher frontal heat flux to the tube deposits was offset by thicker, more insulating frontal deposits so that there was no consistent pattern of temperature relative to angular position.
10. The four alloys (316, 304, 253MA, and 310) tested in both the prior LMF4 test series with Illinois #6 coal and the present LMF5 test series with Montana Rosebud coal showed considerably lower corrosion with the Montana Rosebud coal. The difference was assumed to be due to lower sulfur content in the Rosebud coal and in the tube deposits.

ACKNOWLEDGEMENT

This work was supported by the U. S. Department of Energy, under Contract DE-AC02-79ET10815.

REFERENCES

1. White, M., "Superheater/Intermediate Temperature Airheater Tube Corrosion Tests in the MHD Coal Fired Flow Facility (Eastern Coal Phase)," DOE/ET/10815-208, The Univ. of Tennessee Space Institute, August 1993.
2. Natesan, K., "Materials for Application in MHD Steam Bottoming Plant: Summary Report," Report No. ANL/MHD-84-5, November 1984.
3. Hamer, J. et al, "Micro-alloying Provides Heat and Corrosion Resistance with Leaner alloys," J. of Industrial Heating, August 1985.
4. Van Weele, S., "Fireside Corrosion Testing of Candidate Superheater Tube Alloys, Coatings, and Claddings," Final Report, ORNL/Sub/89-SA187/02, Foster Wheeler Development Corp., Livingston, NJ., August 1991.